

## Two Uniform Tailored Finite Point Schemes for the Two Dimensional Discrete Ordinates Transport Equations with Boundary and Interface Layers

Houde Han<sup>1</sup>, Min Tang<sup>2,\*</sup> and Wenjun Ying<sup>2</sup>

<sup>1</sup> *Department of Mathematical Sciences, Tsinghua University, Haidian, Beijing 100084, P.R. China.*

<sup>2</sup> *Department of Mathematics, Institute of Natural Sciences and MOE-LSC, Shanghai Jiao Tong University, Minhang, Shanghai 200240, P.R. China.*

Received 13 April 2013; Accepted (in revised version) 1 August 2013

Available online 3 December 2013

---

**Abstract.** This paper presents two uniformly convergent numerical schemes for the two dimensional steady state discrete ordinates transport equation in the diffusive regime, which is valid up to the boundary and interface layers. A five-point node-centered and a four-point cell-centered tailored finite point schemes (TFPS) are introduced. The schemes first approximate the scattering coefficients and sources by piecewise constant functions and then use special solutions to the constant coefficient equation as local basis functions to formulate a discrete linear system. Numerically, both methods can not only capture the diffusion limit, but also exhibit uniform convergence in the diffusive regime, even with boundary layers. Numerical results show that the five-point scheme has first-order accuracy and the four-point scheme has second-order accuracy, uniformly with respect to the mean free path. Therefore a relatively coarse grid can be used to capture the two dimensional boundary and interface layers.

**AMS subject classifications:** 65L12, 76N20, 35Q70

**Key words:** Neutron transport equation, discrete ordinates method, tailored finite point method, boundary layers, interface layers.

---

## 1 Introduction

The neutron or radiative transport equation is widely used in nuclear engineering, thermal radiation transport, charged-particle transport and oil-well logging tool design, etc..

---

\*Corresponding author. *Email addresses:* hhan@math.tsinghua.edu.cn (H. Han), tangmin@sjtu.edu.cn (M. Tang), wying@sjtu.edu.cn (W. Ying)

Developing efficient numerical methods for the neutron transport equation has been an active area for decades [22–24].

The solutions of the neutron transport equation depend on space, time, and velocities, which require a lot of computational cost for simulations. The discrete ordinates version of the steady state neutron transport equation is a semi-discretization in velocity. Starting from the discrete ordinates methods, which are among the most popularly used methods in the community, various space discretizations are investigated in the last two decades. For example, the diamond-difference method [24], the characteristic method [3, 7], the discontinuous finite element method [1, 29], the nodal method [2, 23], and so on.

When the average distance between two successive collisions (the mean free path)  $\epsilon$  is small, it is generally impossible to accurately solve the discrete ordinates transport equation in the diffusive regime by optically thin ( $\Delta x \ll \epsilon$ ) meshes, because of limits in computer memory. To approximate the solutions, some macroscopic models have been derived by asymptotic analysis [21], for example, the optically thin limit, the optically thick absorptive limit and the optically thick diffusive limit [22]. Here in this paper, we focus ourselves on the diffusive regime. Two criteria for designing accurate space discretizations for the discrete ordinates transport equation are 1) the order of their truncation error which guarantees the convergence and accuracy in the optically thin regime; 2) the discretization should converge to a discretization of the diffusion limit equation as the mean free path tends to zero [19, 20]. This gives the accuracy with optically thick cell ( $\Delta x \gg \epsilon$ ) of a transport spatial discretization.

The idea of using unresolved cells to capture the macroscopic limit model has been successfully extended to more general applications, which is called asymptotic preserving schemes [8]. However the asymptotic preserving property only guarantees the accuracy of the diffusive region away from the boundary layer. One important issue is the scheme behavior in the presence of unresolved boundary/interface layers. In many applications, if a diffusive region is adjacent to a transport region, boundary and interface layers may appear. Flux changes rapidly across the boundary/interface layers, which requires sufficiently fine grids to capture these changes. It is usually impractical to prescribe a spatial grid that adequately resolves all boundary/interface layers. Therefore, it is desirable to design numerical schemes that are accurate across the boundary/interface layers, even if the spatial grids are not fine enough to resolve the fast variations.

The known schemes for the neutron transport equation that can capture the boundary layers with coarse meshes (meshes that do not resolve the fast variation) are restricted to the one dimensional case. For example, the spectral nodal method proposed in [5, 9], the domain decomposition method in [10] and the micro-macro decomposition method discussed in [25]. These methods are shown to be valid up to the boundary even if the boundary layers exist, but *only in one dimension*. Though higher dimensional extensions have been investigated in [2, 5, 28], the additional approximations for the transverse leakage terms make these higher dimensional extensions no longer able to accurately capture the fast changes in the boundary layers.

The difference between one and high dimensional boundary layer analysis is that,

in one space dimension, the solutions change fast in one direction and it is possible to express the solution by a finite number of basis functions, while in higher dimensions, the solutions vary fast in infinite number of directions and have infinite number of basis functions for the general solutions. This makes the high dimensional boundary layer analysis and simulations much harder than the one dimensional case. To the best of authors' knowledge, there exists no numerical method for the neutron transport equation that can capture the high dimensional boundary and interface layers with coarse meshes [22].

In this paper, we construct two new space discretizations for the two dimensional steady state discrete ordinates transport equation with discontinuous coefficients, which, by using coarse meshes, can capture not only the diffusion limit in the diffusive region but also the fast changes in the boundary/interface layers. The idea is to use the tailored finite point method that was proposed by Han, Huang and Kellogg [15, 16] for the numerical solutions of singular perturbation problems of second order elliptic equations with constant coefficients. The basic idea of the tailored finite point method is that the numerical scheme is tailor-made at each point, based on the local properties of the solutions. Since this method makes full use of the analytical property of the local solutions, it can capture the boundary layers even with coarse grids. Later on, Han and Huang [12–14] and Shih, Kellogg et al. [26, 27] systematically extend this method for the nonhomogeneous reaction-diffusion, convection-diffusion and convection-diffusion-reaction problems.

In this work, we focus on the isotropic scattering case with discontinuous coefficients, where the total cross section, the macroscopic scattering cross section and the neutron source are all isotropic in velocity and piecewise smooth in space. The remainder of this paper is organized as follows. In Section 2, we give a brief introduction of the neutron transport equation, its diffusion limit and the discrete ordinates equations. In Section 3, we discuss about the homogeneous discrete ordinates equations with constant coefficients and its special solutions, which are used as local basis functions in the construction of TFPS. A five-point node-centered TFPS and a four-point cell-centered TFPS, are described in Section 4. In Section 5, some numerical examples are presented to demonstrate their uniform convergence when the boundary/interface layers exist and ability to capture the boundary/interface layers. Finally, we conclude with a discussion in Section 6.

## 2 The two dimensional discrete ordinate transport equation

### 2.1 The two dimensional neutron transport equation

When particles in a bounded domain interact with a background through absorption and scattering processes, the density function is governed by the linear neutron transport equation.

The steady state isotropic neutron transport equation reads [24]:

$$\epsilon \mathbf{u} \cdot \nabla \psi(\mathbf{z}, \mathbf{u}) + \sigma_T(\mathbf{z}) \psi(\mathbf{z}, \mathbf{u}) = \frac{1}{4\pi} \left( \sigma_T(\mathbf{z}) - \epsilon^2 \sigma_a(\mathbf{z}) \right) \int_S \psi(\mathbf{z}, \mathbf{u}) d\mathbf{u} + \epsilon^2 q(\mathbf{z}), \quad (2.1)$$

subject to the boundary conditions

$$\psi(\mathbf{z}, \mathbf{u}) = \psi_\Gamma^-(\mathbf{z}, \mathbf{u}), \quad \text{for } \mathbf{z} \in \Gamma_{\mathbf{u}}^- = \{\mathbf{z} \in \Gamma = \partial\Omega : \mathbf{u} \cdot \mathbf{n}_z < 0\}, \quad \mathbf{u} \in S. \quad (2.2)$$

Here  $\mathbf{z} \in \Omega \subset \mathbb{R}^3$  is the space variable,  $\mathbf{n}_z$  is the outward normal vector and  $S = \{\mathbf{v} | \mathbf{v} \in \mathbb{R}^3, |\mathbf{v}| = 1\}$  represents the directions of particle velocities.  $\psi(\mathbf{z}, \mathbf{u})$  is the density of the particles moving in direction  $\mathbf{u} \in S$  at position  $\mathbf{z}$ .  $\epsilon$  is a dimensionless parameter that is given by the ratio of the mean free path describing the average distance between two successive collisions and the typical length scale. The quantities,  $\sigma_T/\epsilon$ ,  $\epsilon\sigma_a$  and  $\epsilon q$ , are the total cross section, absorption cross section and source respectively, in which  $\sigma_T(\mathbf{z})$ ,  $\sigma_a(\mathbf{z})$  and  $q(\mathbf{z})$  are piecewise smooth whose values are bounded and independent of  $\epsilon$  and the  $L^\infty$  norm of their derivatives  $\nabla\sigma_T(\mathbf{z})$ ,  $\nabla\sigma_a(\mathbf{z})$  and  $\nabla q(\mathbf{z})$  are also bounded and independent of  $\epsilon$ , except at the interfaces.  $\psi_\Gamma^-(\mathbf{z}, \mathbf{u})$  is a given function on  $\Gamma_{\mathbf{u}}^- \times S$ , which specifies the particle densities that come into the computational domain.

Interface conditions are needed to determine the unique solution. Assume that the particles do not change their directions when passing through the interfaces of different media, which indicates that, at the interfaces, the coefficients  $\sigma_T$ ,  $\sigma_a$  and  $q$  may have discontinuities, but  $\psi(\mathbf{z}, \mathbf{u})$  is continuous. For any interface line  $\alpha$ , let the two different media be denoted by  $+$  and  $-$ , we have

$$\psi^+|_\alpha = \psi^-|_\alpha. \quad (2.3)$$

The neutron transport equation (2.1) is a six-dimensional equation in the space variables  $\mathbf{z} \in \mathbb{R}^3$  and directions  $\mathbf{u} \in S$ . It can be reduced to lower dimensional equations. In the Cartesian coordinate system, let

$$\mathbf{u} = (c, s, \zeta)$$

with

$$c = (1 - \zeta^2)^{\frac{1}{2}} \cos\theta \quad \text{and} \quad s = (1 - \zeta^2)^{\frac{1}{2}} \sin\theta \quad \text{for } |\zeta| \leq 1.$$

The neutron transport equation (2.1) has the form

$$\begin{aligned} & \epsilon \left( c \frac{\partial \psi}{\partial x} + s \frac{\partial \psi}{\partial y} + \zeta \frac{\partial \psi}{\partial z} \right) + \sigma_T(x, y, z) \psi \\ &= \frac{1}{4\pi} \left( \sigma_T(x, y, z) - \epsilon^2 \sigma_a(x, y, z) \right) \int_0^{2\pi} \int_{-1}^1 \psi(x, y, z, c, s, \zeta) d\zeta d\theta + \epsilon^2 q(x, y, z). \end{aligned} \quad (2.4)$$

Suppose that  $\sigma_T$ ,  $\sigma_a$ ,  $q$  only depend on  $x$ ,  $y$  and  $\psi$  is uniform along the  $z$  axis. The function

$$\tilde{\psi}(x, y, \zeta, \theta) = \frac{1}{2} [\psi(x, y, z, c, s, \zeta) + \psi(x, y, z, c, s, -\zeta)]$$

is independent of  $z$  and an even function in  $\zeta$ . Eq. (2.4) is reduced to a two space dimensional neutron transport equation

$$\begin{aligned} &\epsilon \left( c \frac{\partial \tilde{\psi}}{\partial x} + s \frac{\partial \tilde{\psi}}{\partial y} \right) + \sigma_T(x,y) \tilde{\psi} \\ &= \frac{1}{2\pi} \left( \sigma_T(x,y) - \epsilon^2 \sigma_a(x,y) \right) \int_0^{2\pi} \int_0^1 \tilde{\psi}(x,y,c,s) d\zeta d\theta + \epsilon^2 q(x,y) \end{aligned} \quad (2.5)$$

for  $\tilde{\psi}(x,y,\zeta,\theta)$ , in which  $c^2 + s^2 \leq 1$ .

In the case that the boundary condition function  $\psi_\Gamma^-(\mathbf{z}, \mathbf{u}) = \psi_\Gamma(\mathbf{z})$  is independent of  $\mathbf{u}$ , when the collisions between particles are frequent ( $\epsilon \rightarrow 0$ ), the solution of (2.1) becomes isotropic in  $\mathbf{u}$  and can be approximated by the solution of the diffusion equation

$$-\nabla \cdot \left( \frac{1}{\sigma_T} \nabla \phi \right) + \sigma_a \phi = q, \quad (2.6)$$

subject to the boundary condition

$$\phi(\mathbf{z}) = \psi_\Gamma, \quad \text{for } \mathbf{z} \in \Gamma. \quad (2.7)$$

In two space dimensions, the diffusion limit equation corresponding to (2.5) takes the form:

$$-\frac{\partial}{\partial x} \left( \frac{2}{3\sigma_T} \frac{\partial \phi}{\partial x} \right) - \frac{\partial}{\partial y} \left( \frac{2}{3\sigma_T} \frac{\partial \phi}{\partial y} \right) + \sigma_a \phi = q. \quad (2.8)$$

The diffusion limit equation can be derived by the Chapman-Enskog expansion as discussed in [21]. The calculations are straightforward and we omit the details here. Note that being isotropic in  $\mathbf{u}$  implies different physical settings in the two transport equation (2.1) and (2.5), which causes the different coefficients in the elliptic operators in (2.6) and (2.8).

## 2.2 The discrete-ordinate transport equations

The idea of the discrete ordinate method is to approximate the integral in the original transport equation (2.4) by numerical quadrature set [24]. In the two dimensional equation (2.5), let the discrete points be  $\{(\zeta_m, \theta_m)\}_{m \in V}$  with weights  $\{w_m\}_{m \in V}$ . Here,  $V$  represents the index set. Let  $c_m = (1 - \zeta_m^2)^{1/2} \cos(\theta_m)$  and  $s_m = (1 - \zeta_m^2)^{1/2} \sin(\theta_m)$  with  $\zeta_m \in [0, 1]$ . We represent the quadrature set by  $\{c_m, s_m, w_m\}_{m \in V}$ .

The discrete-ordinate form of (2.5) by the quadrature set reads

$$\epsilon \left( c_m \frac{\partial}{\partial x} \psi_m + s_m \frac{\partial}{\partial y} \psi_m \right) + \sigma_T \psi_m = (\sigma_T - \epsilon^2 \sigma_a) \sum_{n \in V} \psi_n w_n + \epsilon^2 q, \quad m \in V, \quad (2.9)$$

with  $\psi_m = \psi_m(x,y)$  be an approximation of the density function  $\tilde{\psi}(x,y,\zeta_m,\theta_m)$  for  $m \in V$ . For simplicity, we assume that the spatial variables  $x \in (0,a)$  and  $y \in (0,b)$  with two positive real numbers  $a$  and  $b$ . Let rectangle

$$\mathbf{D} = \{ (x,y) \mid x \in (0,a), y \in (0,b) \}$$

be the computational domain, in which the discrete-ordinate equation (2.9) holds. On the boundary  $\partial\mathbf{D}$ , the approximate particle density functions  $\{\psi_m(x,y)\}_{m \in V}$  satisfy the boundary conditions (2.2), which now take the form, for  $x \in [0,a]$  and  $y \in [0,b]$ ,

$$\psi_m(0,y) = \psi_{Lm}(y), \quad c_m > 0; \quad \psi_m(a,y) = \psi_{Rm}(y), \quad c_m < 0; \quad (2.10a)$$

$$\psi_m(x,0) = \psi_{Bm}(x), \quad s_m > 0; \quad \psi_m(x,b) = \psi_{Tm}(x), \quad s_m < 0. \quad (2.10b)$$

Here,  $\psi_{Bm}(x)$ ,  $\psi_{Tm}(x)$ ,  $\psi_{Lm}(y)$  and  $\psi_{Rm}(y)$  ( $m \in V$ ) are known functions. The interface conditions corresponding to (2.3) become

$$\psi_m^+|_\alpha = \psi_m^-|_\alpha, \quad m \in V. \quad (2.11)$$

In order to have the discrete-ordinate equations (2.9) converge to the same diffusion limit equation (2.8), as  $\epsilon$  tends to zero (when the boundary conditions are independent of  $m$ ), the quadrature set  $\{c_m, s_m, w_m\}_{m \in V}$  is required to satisfy the condition [28]

$$\sum_{n \in V} w_n = 1, \quad \sum_{n \in V} w_n c_n = 0, \quad \sum_{n \in V} w_n s_n = 0, \quad (2.12a)$$

$$\sum_{n \in V} w_n c_n s_n = 0, \quad \sum_{n \in V} w_n (c_n^2 + s_n^2) = \frac{2}{3}. \quad (2.12b)$$

This can be obtained by similar Chapman-Enskog expansions as in the derivation of the diffusion limit equation.

Let  $M$  be a positive integer and  $V = \{1, 2, \dots, 4M\}$  be the index set. We choose a symmetric quadrature set  $\{c_m, s_m, w_m\}$  by assuming

$$w_m = w_{m+M} = w_{m+2M} = w_{m+3M} > 0, \quad m = 1, \dots, M, \quad (2.13a)$$

$$\theta_m = \theta_{m+M} - \frac{\pi}{2} = \theta_{m+2M} - \pi = \theta_{m+3M} - \frac{3}{2}\pi \in \left(0, \frac{\pi}{2}\right), \quad m = 1, \dots, M, \quad (2.13b)$$

$$\zeta_m = \zeta_{m+M} = \zeta_{m+2M} = \zeta_{m+3M} \in [0, 1], \quad m = 1, \dots, M, \quad (2.13c)$$

$$c_m = (1 - \zeta_m^2)^{\frac{1}{2}} \cos \theta_m, \quad s_m = (1 - \zeta_m^2)^{\frac{1}{2}} \sin \theta_m, \quad m \in V. \quad (2.13d)$$

The requirement (2.12) indicates  $\sum_{n=1}^M w_n (1 - \zeta_n^2) = \frac{1}{6}$  and further

$$\sum_{n=1}^M w_n \zeta_n^2 = \frac{1}{12}. \quad (2.14)$$

We can check that when the set  $\{c_m, s_m, w_m\}$  are chosen by (2.13)-(2.14), the requirement (2.12) is satisfied, so that the discrete-ordinate system possesses the same diffusion limit as the original integral equation.

In this paper, we consider the most commonly used Gaussian quadratures set

$$S_N = \{c_m, s_m, w_m\}_{m \in V}$$

with  $N$  a positive integer parameter [24]. In a quadrature set  $S_N$ , each quadrant has  $M = N(N+1)/2$  ordinates and  $N$  distinct  $\zeta_m \in (0,1)$ , which are the positive roots of the standard Legendre polynomial of degree  $2N$  on interval  $[-1,1]$ . We display the corresponding  $c_m, s_m, w_m$  for  $S_1, S_2, S_3, S_4$ . It is easy to check that the Gaussian quadratures satisfy (2.13)-(2.14).

- **Quadrature set  $S_1$ :** When  $N = 1$  and  $M = N(N+1)/2 = 1$ ,  $\zeta_1^2 = 1/3$ ,  $\theta = \pi/4$ , then

$$\begin{aligned} (c_{1,s_1}) &= \left(\frac{\sqrt{3}}{3}, \frac{\sqrt{3}}{3}\right), & (c_{2,s_2}) &= \left(\frac{-\sqrt{3}}{3}, \frac{\sqrt{3}}{3}\right), \\ (c_{3,s_3}) &= \left(-\frac{\sqrt{3}}{3}, -\frac{\sqrt{3}}{3}\right), & (c_{4,s_4}) &= \left(\frac{\sqrt{3}}{3}, -\frac{\sqrt{3}}{3}\right), \\ w_1 = w_2 = w_3 = w_4 &= \frac{1}{4}. \end{aligned}$$

- **Quadrature set  $S_2$ :** When  $N = 2$  and  $M = N(N+1)/2 = 3$ , the quadrature nodes and weights of the quadrature set  $S_2$  are presented in Table 1.

Table 1: The nodes and weights of the quadrature set  $S_2$ .

$\zeta_m$	$\theta_m$	$c_m$	$s_m$	$4w_m$
0.3399810	$\pi/8$	0.8688461	0.3598879	0.3260726
0.3399810	$3\pi/8$	0.3598879	0.8688461	0.3260726
0.8611363	$\pi/4$	0.3594748	0.3594748	0.3478548

- **Quadrature set  $S_3$ :** When  $N = 3$  and  $M = N(N+1)/2 = 6$ , the quadrature nodes and weights of the quadrature set  $S_3$  are presented in Table 2.

Table 2: The nodes and weights of the quadrature set  $S_3$ .

$\zeta_m$	$\theta_m$	$c_m$	$s_m$	$4w_m$
0.2386192	$\pi/12$	0.9380233	0.2513426	0.1559713
0.2386192	$3\pi/12$	0.6866807	0.6866807	0.1559713
0.2386192	$5\pi/12$	0.2513426	0.9380233	0.1559713
0.6612094	$\pi/8$	0.6930957	0.2870896	0.1803808
0.6612094	$3\pi/8$	0.2870896	0.6930957	0.1803808
0.9324695	$\pi/4$	0.2554414	0.2554414	0.1713245

- **Quadrature set  $S_4$ :** When  $N = 4$  and  $M = N(N+1)/2 = 10$ , the quadrature nodes and weights of quadrature set  $S_4$  are presented in Table 3.

Table 3: The nodes and weights of the quadrature set  $S_4$ .

$\zeta_m$	$\theta_m$	$c_m$	$s_m$	$4\tau w_m$
0.1834346	$\pi/16$	0.9641432	0.1917800	0.0906709
0.1834346	$3\pi/16$	0.8173612	0.5461433	0.0906709
0.1834346	$5\pi/16$	0.5461433	0.8173612	0.0906709
0.1834346	$7\pi/16$	0.1917800	0.9641432	0.0906709
0.5255324	$\pi/12$	0.8217842	0.2201964	0.1045689
0.5255324	$3\pi/12$	0.6015878	0.6015878	0.1045689
0.5255324	$5\pi/12$	0.2201964	0.8217842	0.1045689
0.7966665	$\pi/8$	0.5584105	0.2313012	0.1111905
0.7966665	$3\pi/8$	0.2313012	0.5584105	0.1111905
0.9602899	$\pi/4$	0.1972858	0.1972858	0.1012285

$S_N$  ( $N=1,2,3,4$ ) satisfy not only the requirement (2.13)-(2.14), but also

$$w_m = w_{M-m}, \quad \theta_m + \theta_{M-m} = \frac{\pi}{2}, \quad m = 1, \dots, M, \quad (2.15)$$

which introduces additional symmetries.

### 3 Special solutions to homogeneous constant coefficients system

In order to apply the tailored finite point method to construct numerical schemes for the boundary value problem (2.9)-(2.11) with variable coefficients, we need to use the special solutions to the problem of interest as basis functions. In this section, we will find the special solutions to the homogeneous discrete-ordinate equations

$$\epsilon \left( c_m \frac{\partial}{\partial x} + s_m \frac{\partial}{\partial y} \right) \psi_m + \sigma_T \psi_m = (\sigma_T - \epsilon^2 \sigma_a) \sum_{n \in V} \omega_n \psi_n, \quad m \in V, \quad (3.1)$$

with constant coefficients  $\sigma_T$  and  $\sigma_a$ .

Let

$$\mathbf{\Psi}(\mathbf{x}) = (\psi_1(\mathbf{x}), \psi_2(\mathbf{x}), \dots, \psi_{4M}(\mathbf{x}))^T \in \mathbb{R}^{4M}$$

with  $\mathbf{x} = (x, y) \in \mathbb{R}^2$ . Now we introduce an auxiliary function

$$C(\mathbf{x}) = \sum_{n \in V} \omega_n \psi_n(\mathbf{x})$$

and rewrite system (3.1) in the following form

$$\begin{pmatrix} \mathbf{L} & \mathbf{0} \\ \mathbf{0} & \mathbf{1} \end{pmatrix} \begin{pmatrix} \mathbf{\Psi}(\mathbf{x}) \\ C(\mathbf{x}) \end{pmatrix} = \begin{pmatrix} \mathbf{0} & \mathbf{e} \\ \mathbf{w}^T & \mathbf{0} \end{pmatrix} \begin{pmatrix} \mathbf{\Psi}(\mathbf{x}) \\ C(\mathbf{x}) \end{pmatrix}. \quad (3.2)$$

Here,  $\mathbf{L}$  is a  $4M$  by  $4M$  diagonal matrix, whose  $m^{th}$  diagonal entry reads  $\epsilon(c_m\partial_x + s_m\partial_y) + \sigma_T$ , for  $m \in V$ , and vectors  $\mathbf{e}, \mathbf{w} \in \mathbb{R}^{4M \times 1}$  are respectively given by

$$\mathbf{e} = (\sigma_T - \epsilon^2\sigma_a)(1, 1, \dots, 1)^T$$

and

$$\mathbf{w} = (w_1, w_2, \dots, w_{4M})^T.$$

The system (3.2) contains  $(4M+1)$  unknown functions  $\Psi(\mathbf{z})$  and  $C(\mathbf{z})$ .

The two systems (3.1) and (3.2) are equivalent to each other. In the subsequent part, we are going to find special solutions of the form

$$\begin{pmatrix} \Psi(\mathbf{z}) \\ C(\mathbf{z}) \end{pmatrix} = \begin{pmatrix} \xi \\ \eta \end{pmatrix} \exp\left\{\frac{\lambda x + \mu y}{\epsilon}\right\} \tag{3.3}$$

to the system (3.2), then the corresponding special solutions to (3.1).

In order to determine the nonzero vector  $\xi = (\xi_1, \xi_2, \dots, \xi_{4M})^T$  and scalar constant  $\eta$  as well as  $\lambda$  and  $\mu$ , we substitute (3.3) into (3.2). Finding a special solution of the form (3.3) reduces to a matrix eigenvalue problem: find  $\lambda, \mu \in \mathbb{C}$  and nonzero vector  $(\xi, \eta) \in \mathbb{C}^{4M} \times \mathbb{C}$  such that

$$\begin{pmatrix} \mathbf{A} & 0 \\ 0 & 1 \end{pmatrix} \begin{pmatrix} \xi \\ \eta \end{pmatrix} = \begin{pmatrix} 0 & \mathbf{e} \\ \mathbf{w}^T & 0 \end{pmatrix} \begin{pmatrix} \xi \\ \eta \end{pmatrix}. \tag{3.4}$$

Here,  $\mathbf{A} = \mathbf{A}(\lambda, \mu)$  is a  $4M$  by  $4M$  diagonal matrix, whose  $m^{th}$  diagonal entry reads  $c_m\lambda + s_m\mu + \sigma_T$ , for  $m \in V$ . We define  $(\lambda, \mu)$  as an eigenvalue pair of the problem, if there exists nonzero solution  $(\xi, \eta)^T$  to the system (3.4).

### The eigenvalue pairs

Note that the eigenvalue pair  $(\lambda, \mu)$  is a zero point of the characteristic polynomial:

$$\begin{aligned} p_{4M}(\lambda, \mu) &\equiv \det \begin{pmatrix} \mathbf{A}(\lambda, \mu) & -\mathbf{e} \\ -\mathbf{w}^T & 1 \end{pmatrix} \\ &= \prod_{m \in V} (c_m\lambda + s_m\mu + \sigma_T) - (\sigma_T - \epsilon^2\sigma_a) \sum_{n \in V} \left[ \omega_n \prod_{m \neq n} (c_m\lambda + s_m\mu + \sigma_T) \right]. \end{aligned} \tag{3.5}$$

We have either

$$\pi_{4M}(\lambda, \mu) \equiv \prod_{m \in V} (c_m\lambda + s_m\mu + \sigma_T) = 0, \tag{3.6}$$

or

$$q_{4M}(\lambda, \mu) \equiv 1 - \sum_{n \in V} \frac{\omega_n(\sigma_T - \epsilon^2\sigma_a)}{c_n\lambda + s_n\mu + \sigma_T} = 0. \tag{3.7}$$

A few characteristic curves when  $\epsilon = 0.1$  for  $p_{4M}(\lambda, \mu)$  with  $M = 1, 3, 6, 10$  are shown in Fig. 1, where the horizontal and vertical axes represent respectively  $\lambda$  and  $\mu$ . A point on the curves corresponds to an eigenvalue pair  $(\lambda, \mu)$ . Only those eigenvalue pairs of which both  $\lambda$  and  $\mu$  are real numbers are plotted.

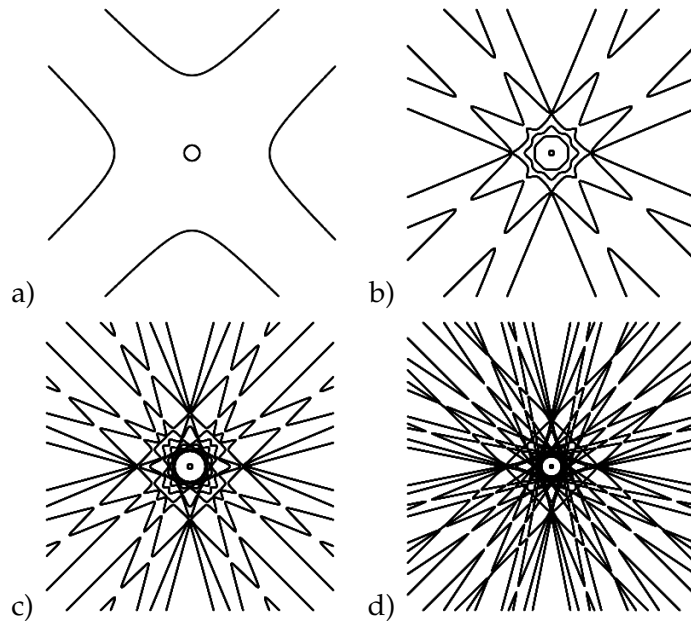


Figure 1: Characteristic curves when  $\epsilon = 0.1$ : (a)  $M = 1$ ; (b)  $M = 3$ ; (c)  $M = 6$ ; (d)  $M = 10$ .

**The eigenvectors corresponding to  $(\lambda, \mu)$**

After  $(\lambda, \mu)$  is determined, we have to find the eigenvector  $(\xi, \eta)$  associated with the eigenvalue pair.

From Eq. (3.4), we get

$$\begin{cases} (c_m \lambda + s_m \mu + \sigma_T) \xi_m = (\sigma_T - \epsilon^2 \sigma_a) \eta, & \forall m \in V, \\ \eta = \sum_{n \in V} \omega_n \xi_n. \end{cases} \tag{3.8}$$

Case 1. Suppose that  $c_m \lambda + s_m \mu + \sigma_T \neq 0$  for all  $m \in V$ , then we get

$$\begin{cases} \xi_m = \frac{\sigma_T - \epsilon^2 \sigma_a}{c_m \lambda + s_m \mu + \sigma_T}, & \forall m \in V, \\ \eta = 1, \end{cases} \tag{3.9}$$

which is an eigenvector associated with the eigenvalue pair  $(\lambda, \mu)$ .

Case 2. There is at least one  $m_1 \in V$  such that

$$c_{m_1} \lambda + s_{m_1} \mu + \sigma_T = 0.$$

Then from (3.8), we obtain

$$\eta = 0,$$

and further

$$(c_m\lambda + s_m\mu + \sigma_T)\zeta_m = 0, \quad \forall m \in V, \tag{3.10a}$$

$$\sum_{n \in V} \omega_n \zeta_n = 0. \tag{3.10b}$$

By Eq. (3.10a), we know that for any  $m \in V$ , we have either  $\zeta_m = 0$  or  $c_m\lambda + s_m\mu + \sigma_T = 0$ . Since  $\zeta$  is nonzero and satisfies (3.10b), there exists another  $m_2 \in V$  such that

$$\zeta_{m_2} \neq 0.$$

This further indicates that

$$c_{m_2}\lambda + s_{m_2}\mu + \sigma_T = 0.$$

Assume that  $(c_{m_1}, s_{m_1})$  and  $(c_{m_2}, s_{m_2})$  are linearly independent and

$$c_m\lambda + s_m\mu + \sigma_T \neq 0, \quad \forall m \neq m_1, m_2. \tag{3.11}$$

Then the components of the eigenvector  $(\zeta, \eta)$  are given by

$$\zeta_m = \begin{cases} 0 & \text{for } m \neq m_1, m_2, \\ w_{m_2} & \text{for } m = m_1, \\ -w_{m_1} & \text{for } m = m_2, \end{cases} \tag{3.12}$$

and

$$\eta = 0. \tag{3.13}$$

Now it is clear that after an eigenvalue pair (a zero point  $(\lambda, \mu)$  of (3.5)) is found, the corresponding eigenvector  $(\zeta, \eta)$  can be obtained directly.

### Properties of the eigenvalue pairs and eigenvectors

We have found infinite number of special solutions in the form (3.3), while the idea of the tailored finite point method is to select a finite number of special solutions and make the discrete scheme satisfy them exactly. We prove in the subsequent part some properties of the eigenvalue pairs and their corresponding eigenvectors, which are crucial in the selection of special solutions.

**Lemma 3.1.** *Suppose that  $\{m_k\}_{k=1}^M$  and  $\{n_k\}_{k=1}^M$  are two permutations of the index set  $\{m\}_{m=1}^M$  such that the directions  $\{c_m, s_m\}_{m=1}^M$  are ordered in the following way*

$$c_{m_1} > c_{m_2} > \dots > c_{m_M} > 0$$

and

$$s_{n_1} > s_{n_2} > \dots > s_{n_M} > 0.$$

The characteristic polynomial  $p_{4M}(\lambda, \mu)$  has  $4M$  distinct roots (eigenvalues) on each of the coordinate axes of the  $\lambda\mu$ -plane. The eigenvalues pairs have the following properties:

i) On the horizontal axis, the  $2M$  distinct positive eigenvalues are given by

$$0 < \lambda_{m_{\frac{1}{2}}} < \lambda_{m_1} < \lambda_{m_{\frac{3}{2}}} < \lambda_{m_2} < \dots < \lambda_{m_{M-\frac{1}{2}}} < \lambda_{m_M}$$

with  $\lambda_{m_k} = \frac{\sigma_T}{c_{m_k}}$  and  $m_{k-\frac{1}{2}} \in \{M+1, \dots, 2M\}$ , for  $k = 1, \dots, M$ . Let  $\lambda_{m_0} = 0$ . The  $2M$  negative distinct eigenvalues are  $\lambda_{2M+m_k} = -\lambda_{m_k}$  for  $k = \frac{1}{2}, 1, \frac{3}{2}, \dots, M$ . The corresponding eigenvectors are given by

$$\xi_{m,l} = \begin{cases} 1, & l = 2M - m, \\ -1, & l = 2M + m, \\ 0, & l \in \{1, \dots, 4M\} / \{2M - m, 2M + m\}, \end{cases} \quad \eta_m = 0,$$

for  $m = m_1, m_2, \dots, m_M, 2M + m_1, \dots, 2M + m_M$  and

$$\xi_{m,l} = \frac{1}{c_l \lambda_m + \sigma_T}, \quad l \in \{1, \dots, 4M\}, \quad \eta_m = 1,$$

for  $m = m_{\frac{1}{2}}, m_{\frac{3}{2}}, \dots, m_{M-\frac{1}{2}}, 2M + m_{\frac{1}{2}}, \dots, 2M + m_{M-\frac{1}{2}}$ .

ii) On the vertical axis, the  $2M$  distinct positive eigenvalues are given by

$$0 < \mu_{n_{\frac{1}{2}}} < \mu_{n_1} < \mu_{n_{\frac{3}{2}}} < \mu_{n_2} < \dots < \mu_{n_{M-\frac{1}{2}}} < \mu_{n_M}$$

with  $\mu_{n_k} = \frac{\sigma_T}{s_{n_k}}$  and  $n_{k-\frac{1}{2}} \in \{M+1, \dots, 2M\}$  for  $k = 1, \dots, M$ . Let  $\mu_{n_0} = 0$ . The  $2M$  negative distinct eigenvalues are  $\mu_{2M+n_k} = -\mu_{n_k}$  for  $k = \frac{1}{2}, 1, \frac{3}{2}, \dots, M$ . The corresponding eigenvectors are given by

$$\xi_{n,l} = \begin{cases} 1, & l = 2M + n, \\ -1, & l = 4M - n, \\ 0, & l \in \{1, \dots, 4M\} / \{2M + n, 4M - n\}, \end{cases} \quad \eta_n = 0,$$

for  $n = n_1, n_2, \dots, n_M, 2M + n_1, \dots, 2M + n_M$ , and

$$\xi_{n,l} = \frac{1}{c_l \lambda_n + \sigma_T}, \quad l \in \{1, \dots, 4M\}, \quad \eta_n = 1,$$

for  $n = n_{\frac{1}{2}}, n_{\frac{3}{2}}, \dots, n_{M-\frac{1}{2}}, 2M + n_{\frac{1}{2}}, \dots, 2M + n_{M-\frac{1}{2}}$ .

iii) When there exist  $4M$  distinct real eigenvalue pairs  $(\lambda_m, \mu_m)$  of the characteristic polynomial (3.5) that satisfy  $\mu_m = \alpha \lambda_m$  with  $\alpha$  some constant, the eigenvectors  $\xi_m$  ( $m \in V$ ) that correspond to these eigenvalue pairs are linearly independent.

*Proof.* i) First of all, the characteristic polynomial (3.5) can be written as

$$p_{4M}(\lambda, \mu) = q_{4M}(\lambda, \mu) \prod_{m \in V} (c_m \lambda + s_m \mu + \sigma_T) = q_{4M}(\lambda, \mu) \pi_{4M}(\lambda, \mu),$$

where  $\pi_{4M}(\lambda, \mu)$  and  $q_{4M}(\lambda, \mu)$  are defined in (3.6) and (3.7), respectively. By the selection of the quadrature set  $\{c_m, s_m, w_m\}_{m \in V}$ , function  $\pi_{4M}(\lambda, \mu)$  has the form

$$\pi_{4M}(\lambda, \mu) = \prod_{m=1}^M \left\{ \left[ \sigma_T^2 - (c_m \lambda + s_m \mu)^2 \right] \left[ \sigma_T^2 - (c_m \lambda - s_m \mu)^2 \right] \right\},$$

and function  $q_{4M}(\lambda, \mu)$  has the form

$$q_{4M}(\lambda, \mu) = 1 - (\sigma_T - \epsilon^2 \sigma_a) \sum_{m=1}^M \left\{ \frac{2\sigma_T w_m}{\sigma_T^2 - (c_m \lambda + s_m \mu)^2} + \frac{2\sigma_T w_m}{\sigma_T^2 - (c_m \lambda - s_m \mu)^2} \right\}.$$

On the horizontal axis of the  $\lambda\mu$ -plane, i.e., when  $\mu = 0$ , we have

$$q_{4M}(\lambda, 0) = 1 - (\sigma_T - \epsilon^2 \sigma_a) \sum_{m=1}^M \frac{4\sigma_T w_m}{\sigma_T^2 - c_m^2 \lambda^2}.$$

From the previous expressions for  $\pi_{4M}(\lambda, \mu)$  and  $q_{4M}(\lambda, \mu)$ , we see that  $\lambda_m^* = \sigma_T / c_m$  and  $\lambda_{m+M}^* = -\sigma_T / c_m$  with  $m = 1, 2, \dots, M$  are  $2M$  distinct zeros/roots of the characteristic polynomial  $p_{4M}(\lambda, \mu)$ . Here, we used the fact that  $\{c_m\}_{m=1}^M$  are distinct by the selection of the quadrature set. Moreover, by the assumption on  $\{c_{m_k}\}_{k=1}^M$ , eigenvalues  $\{\lambda_m^*\}_{m=1}^M$  have the following ordering

$$0 < \lambda_{m_1}^* < \lambda_{m_2}^* < \dots < \lambda_{m_M}^*.$$

Note that function  $q_{4M}(\lambda, \mu)$  tends to negative infinity on the left side of  $\lambda_{m_k}^*$  and tends to positive infinity on the right side of  $\lambda_{m_k}^*$  for each  $k \in \{1, 2, \dots, M\}$ . This means that there is at least a root/zero of the characteristic polynomial between two consecutive  $\lambda_{m_k}^*$ . In addition, at the origin, we have  $q_{4M}(0, 0) = \epsilon^2 \sigma_a / \sigma_T > 0$  while  $q_{4M}(\lambda_{m_1}^*, 0)$  tends to negative infinity. This indicates there is also a root between 0 and  $\lambda_{m_1}^*$ . By symmetry, on the horizontal axis of the  $\lambda\mu$ -plane, there are at least  $2M$  more roots/zeros in addition to  $\{\lambda_m^*\}_{m=1}^{2M}$ . The additional roots interleave with  $\{\lambda_m^*\}_{m=1}^{2M}$ . In this way, we found all  $4M$  roots of the characteristic polynomial  $p_{4M}(\lambda, \mu)$  on the horizontal axis; there is exactly one root in the interval  $(\lambda_{m_{k-1}}^*, \lambda_{m_k}^*)$  and exactly one root in the interval  $(-\lambda_{m_k}^*, -\lambda_{m_{k-1}}^*)$  for each  $k \in \{1, 2, \dots, M\}$ .

ii) Similar discussions in i) hold for  $\mu$ .

iii) When there exist  $4M$  distinct real eigenvalue pairs  $(\lambda_m, \mu_m)$  satisfy  $\mu_m = \alpha \lambda_m$ , we prove the linear independence of the eigenvectors by contradiction. First of all, from the discussions about the eigenvectors, we know that when the quadrature sets are chosen properly, i.e. (3.11) are satisfied for each pair of  $(c_{m_1}, s_{m_1}), (c_{m_2}, s_{m_2})$ , for given  $(\lambda, \mu)$ , there is a unique solution  $(\xi^T, \eta)^T$  to the system (3) (up to the multiplication of a constant).

Assume the  $4M$  distinct eigenvalue pairs are  $(\lambda_1, \alpha \lambda_1), \dots, (\lambda_{4M}, \alpha \lambda_{4M})$  and their corresponding eigenvectors are  $(\xi_1^T, \eta_1)^T, \dots, (\xi_{4M}^T, \eta_{4M})^T$ . If  $\xi_1, \dots, \xi_{4M}$  are linearly dependent, there exist  $(\alpha_1, \dots, \alpha_{4M}) \neq 0$  such that

$$\alpha_1 \xi_1 + \alpha_2 \xi_2 + \dots + \alpha_{4M} \xi_{4M} = 0.$$

Since  $\eta = \mathbf{w}^T \xi$ , we have

$$\alpha_1 \eta_1 + \alpha_2 \eta_2 + \dots + \alpha_{4M} \eta_{4M} = \mathbf{w}^T (\alpha_1 \xi_1 + \alpha_2 \xi_2 + \dots + \alpha_{4M} \xi_{4M}) = 0.$$

The matrix eigenvalue problem (3.4) can be rewritten as

$$\begin{pmatrix} \mathbf{A} - \sigma_T I & 0 \\ 0 & 1 \end{pmatrix} \begin{pmatrix} \xi \\ \eta \end{pmatrix} = \begin{pmatrix} -\sigma_T I & \mathbf{e} \\ \mathbf{w}^T & 0 \end{pmatrix} \begin{pmatrix} \xi \\ \eta \end{pmatrix},$$

with  $I$  the  $4M$  by  $4M$  identity matrix. Then

$$\begin{aligned} & \alpha_1 \begin{pmatrix} \mathbf{B} \lambda_1 & 0 \\ 0 & 1 \end{pmatrix} \begin{pmatrix} \xi_1 \\ \eta_1 \end{pmatrix} + \dots + \alpha_{4M} \begin{pmatrix} \mathbf{B} \lambda_{4M} & 0 \\ 0 & 1 \end{pmatrix} \begin{pmatrix} \xi_{4M} \\ \eta_{4M} \end{pmatrix} \\ &= \begin{pmatrix} \mathbf{B} (\alpha_1 \lambda_1 \xi_1 + \dots + \alpha_{4M} \lambda_{4M} \xi_{4M}) \\ \alpha_1 \eta_1 + \dots + \alpha_{4M} \eta_{4M} \end{pmatrix} \\ &= \begin{pmatrix} -\sigma_T I & \mathbf{e} \\ \mathbf{w}^T & 0 \end{pmatrix} \left( \alpha_1 \begin{pmatrix} \xi_1 \\ \eta_1 \end{pmatrix} + \dots + \alpha_{4M} \begin{pmatrix} \xi_{4M} \\ \eta_{4M} \end{pmatrix} \right) \\ &= 0, \end{aligned}$$

with  $\mathbf{B} = \text{diag}\{c_1 + \alpha s_1, \dots, c_{4M} + \alpha s_{4M}\}$ . Because  $\mathbf{B}$  is a nonsingular matrix, we get

$$\alpha_1 \lambda_1 \xi_1 + \dots + \alpha_{4M} \lambda_{4M} \xi_{4M} = 0.$$

If we further consider  $(\lambda_1 \xi_1^T, \lambda_1 \eta_1)^T, \dots, (\lambda_{4M} \xi_{4M}^T, \lambda_{4M} \eta_{4M})^T$  as the corresponding eigenvectors, similar discussions can give

$$\alpha_1 \lambda_1^2 \xi_1 + \dots + \alpha_{4M} \lambda_{4M}^2 \xi_{4M} = 0.$$

Repeating the above process, we find the following system

$$\begin{pmatrix} \xi_1, \dots, \xi_{4M} \end{pmatrix} \text{diag}\{\alpha_1, \dots, \alpha_{4M}\} \begin{pmatrix} 1 & \lambda_1 & \dots & \lambda_1^{4M} \\ 1 & \lambda_2 & \dots & \lambda_2^{4M} \\ \vdots & \vdots & \vdots & \vdots \\ 1 & \lambda_{4M} & \dots & \lambda_{4M}^{4M} \end{pmatrix} = 0. \tag{3.14}$$

The third matrix on the left hand side in (3.14) is nonsingular, thanks to that  $\lambda_1, \dots, \lambda_{4M}$  are different from each other. Moreover,  $\xi_1, \dots, \xi_{4M}$  are nonzero, we get

$$(\alpha_1, \dots, \alpha_{4M}) = 0,$$

which is a contradiction, the proof is concluded. □

**Remark 3.1.** The auxiliary function  $C(\mathbf{z})$  satisfies a high-order partial differential equation

$$\begin{aligned} & \prod_{m \in V} \left( \epsilon c_m \frac{\partial}{\partial x} + \epsilon s_m \frac{\partial}{\partial y} + \sigma_T \right) C(\mathbf{z}) \\ & - (\sigma_T - \epsilon^2 \sigma_a) \sum_{n \in V} \left[ \omega_n \prod_{m \neq n} \left( \epsilon c_m \frac{\partial}{\partial x} + \epsilon s_m \frac{\partial}{\partial y} + \sigma_T \right) \right] C(\mathbf{z}) = 0. \end{aligned}$$

## 4 Two tailored finite point schemes

In this section, we construct two tailored finite point schemes for the boundary value problem (2.9)-(2.10) on the rectangular domain  $\mathbf{D}$ . We call the first one as a five-point node-centered scheme since the TFPS stencil at each grid node involves five adjacent grid nodes; the second one as a four-point cell-centered scheme since each equation in the resulting discrete TFPS involves four points, which are the edge centers of a grid cell.

The derivations of these two schemes are similar, but the idea is different. The node-centered scheme inherits the view of the finite point method as those discussed in [12, 13, 16], while the idea of the cell-centered scheme is close to the finite element method, in each cell, the approximate solution is given by the basis functions, using which, we can piece together the numerical solution with the neighboring cells by the interface conditions. Therefore, it is more appropriate for interface problems. We will see the differences more clearly in the numerical examples.

On the rectangular domain  $\Omega = [0, a] \times [0, b]$ , we have the grid nodes

$$\mathbf{z}_{i,j} = (x_i, y_j), \quad i = 0, 1, \dots, I \quad \text{and} \quad j = 0, 1, \dots, J.$$

Here  $I$  and  $J$  are two positive integers. Let  $h_1 = a/I$  and  $h_2 = b/J$  be two mesh parameters,  $x_i = ih_1$  with  $i = 0, 1, \dots, I$  and  $y_j = jh_2$  with  $j = 0, 1, \dots, J$ .

### 4.1 The five-point node-centered scheme

For each interior grid node  $\mathbf{z}_{i,j}$ , which is not on the domain boundary, let

$$E_{i,j} = \{ (x, y) \mid |x - x_i| \leq h_1, |y - y_j| \leq h_2 \}$$

be the rectangular patch centered at  $\mathbf{z}_{i,j}$ . The four adjacent grid nodes  $\{\mathbf{z}_{i+1,j}, \mathbf{z}_{i,j+1}, \mathbf{z}_{i-1,j}, \mathbf{z}_{i,j-1}\}$  are on the boundary of patch  $E_{i,j}$ .

We may assume that the coefficients,  $\sigma_T$ ,  $\sigma_a$  and  $q$ , are constants in each patch  $E_{i,j}$ . Otherwise, for equations with variable but smooth coefficients, we choose the values for  $\sigma_T$ ,  $\sigma_a$  and  $q$  by their local averages on  $E_{i,j}$ .

That is, we assume the discrete ordinates equations (2.9) on  $E_{i,j}$  is approximated by the following first order partial differential equations with constant coefficients

$$\epsilon \left( c_m \frac{\partial}{\partial x} \tilde{\psi}_m + s_m \frac{\partial}{\partial y} \tilde{\psi}_m \right) + \sigma_T \tilde{\psi}_m = \epsilon^2 q + (\sigma_T - \epsilon^2 \sigma_a) \sum_{n \in V} \omega_n \tilde{\psi}_n, \quad \text{for } m \in V. \quad (4.1)$$

Let  $\mathbf{\Psi}^{(0)} = (\psi_1^{(0)}, \dots, \psi_{4M}^{(0)})^T = \frac{q}{\sigma_a} (1, 1, \dots, 1)^T \in \mathbb{R}^{4M}$ . It is straightforward to check that  $\mathbf{\Psi}^{(0)}$  is a particular solution of Eq. (4.1), and the difference  $\mathbf{\Psi}(\mathbf{z}) = \tilde{\mathbf{\Psi}}(\mathbf{z}) - \mathbf{\Psi}^{(0)}$  satisfies the homogeneous equations

$$\epsilon \left( c_m \frac{\partial}{\partial x} \psi_m + s_m \frac{\partial}{\partial y} \psi_m \right) + \sigma_T \psi_m = (\sigma_T - \epsilon^2 \sigma_a) \sum_{n \in V} \omega_n \psi_n, \quad \text{for } m \in V. \quad (4.2)$$

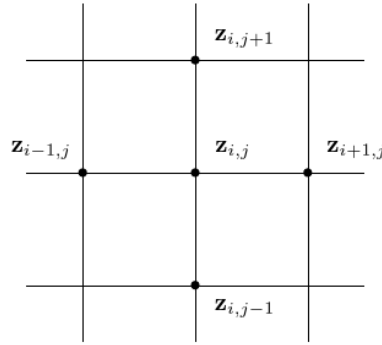


Figure 2: TFPM stencil for the five-point node-centered scheme.

Let  $K$  be a positive integer. We consider  $K$  linearly independent special solutions to the system (4.2) that have the form

$$\Psi^{(k)}(\mathbf{z}) = \xi^{(k)} \exp \left\{ \frac{\lambda_k(x - x_i) + \mu_k(y - y_j) - \max\{h_1|\lambda_k|, h_2|\mu_k|\}}{\epsilon} \right\}, \tag{4.3}$$

for  $k=1, 2, \dots, K$ . Here, as discussed in Section 3,  $(\lambda_k, \mu_k)$  is a real eigenvalue pair of system (4.2) and  $\xi^{(k)}$  is the eigenvector associated with  $(\lambda_k, \mu_k)$ , for  $k=1, 2, \dots, K$ .

**Remark 4.1.** (4.3) is the same as (3.3) but subtracting  $(\lambda_k x_i + \mu_k y_j + \max\{h_1|\lambda_k|, h_2|\mu_k|\})/\epsilon$  in the power of the exponential, which is equivalent to multiplying some constant in the basis. We are interested in problems with wide ranges of mean free path, the constant subtracting in the exponential of (4.3) is to avoid overflow when  $\epsilon$  is small during computation. Since when  $\epsilon$  is small, different choices of  $\lambda_k, \mu_k$  contain the information of different layers, special solutions of the form (4.3) or (3.3) are crucial in constructing the TFPS.

Let  $\{\alpha_k, k=1, 2, \dots, K\}$  be constants, the vector-valued function

$$\tilde{\Psi}(\mathbf{z}) = \Psi^{(0)} + \sum_{k=1}^K \alpha_k \Psi^{(k)}(\mathbf{z}) \tag{4.4}$$

is a solution to the nonhomogeneous system (4.1).

For each patch  $E_{i,j}$ , we choose four points

$$\{\mathbf{z}_{i+1,j}, \mathbf{z}_{i,j+1}, \mathbf{z}_{i-1,j}, \mathbf{z}_{i,j-1}\}$$

on the boundary together with the center  $\mathbf{z}_{i,j}$  to construct the five-point node-centered scheme for the local problem around  $\mathbf{z}_{i,j}$ .

The discrete in-flow boundary conditions for (4.1) are given by the  $K = 4 \times (4M/2) = 8M$  values at the four grid points  $(\mathbf{z}_{i+1,j}, \mathbf{z}_{i,j+1}, \mathbf{z}_{i-1,j}, \mathbf{z}_{i,j-1})$ :

$$\begin{cases} \tilde{\psi}_m(\mathbf{z}_{i+1,j}), & \text{with } c_m < 0, \\ \tilde{\psi}_m(\mathbf{z}_{i,j+1}), & \text{with } s_m < 0, \\ \tilde{\psi}_m(\mathbf{z}_{i-1,j}), & \text{with } c_m > 0, \\ \tilde{\psi}_m(\mathbf{z}_{i,j-1}), & \text{with } s_m > 0, \end{cases} \quad (4.5)$$

for  $m \in V$ . Then the constants  $\{\alpha_k, k = 1, 2, \dots, K\}$  in (4.4) are determined by the boundary conditions (4.5), namely, for  $m \in V$ ,

$$\begin{cases} \psi_m^{(0)} + \sum_{k=1}^K \alpha_k \psi_m^{(k)}(\mathbf{z}_{i+1,j}) = \tilde{\psi}_m(\mathbf{z}_{i+1,j}), & \text{with } c_m < 0, \\ \psi_m^{(0)} + \sum_{k=1}^K \alpha_k \psi_m^{(k)}(\mathbf{z}_{i,j+1}) = \tilde{\psi}_m(\mathbf{z}_{i,j+1}), & \text{with } s_m < 0, \\ \psi_m^{(0)} + \sum_{k=1}^K \alpha_k \psi_m^{(k)}(\mathbf{z}_{i-1,j}) = \tilde{\psi}_m(\mathbf{z}_{i-1,j}), & \text{with } c_m > 0, \\ \psi_m^{(0)} + \sum_{k=1}^K \alpha_k \psi_m^{(k)}(\mathbf{z}_{i,j-1}) = \tilde{\psi}_m(\mathbf{z}_{i,j-1}), & \text{with } s_m > 0. \end{cases} \quad (4.6)$$

This is a system of  $8M$  linear algebraic equations and the coefficients  $\{\alpha_k\}_{k=1}^K$  can be determined by (4.5). Moreover, from (4.4), at the point  $\mathbf{z}_{i,j}$ ,

$$\tilde{\Psi}(\mathbf{z}_{i,j}) = \Psi^{(0)} + \sum_{k=1}^K \alpha_k \Psi^{(k)}(\mathbf{z}_{i,j}). \quad (4.7)$$

If we express the constants  $\{\alpha_k, k = 1, 2, \dots, K\}$  by the unknowns in (4.5) through solving (4.6), (4.7) becomes a finite difference scheme that connects the unknowns at the grid node  $\mathbf{z}_{i,j}$  with those at the four adjacent grid nodes. This is the five-point node-centered TFPS for the discrete ordinates equation.

**Remark 4.2.** If one of the grid nodes  $\{\mathbf{z}_{i+1,j}, \mathbf{z}_{i,j+1}, \mathbf{z}_{i-1,j}, \mathbf{z}_{i,j-1}\}$  is on the physical boundary  $\partial\mathbf{D}$  of the computational domain, we simply replace the corresponding component values  $\tilde{\psi}_m$  with the physical boundary conditions (2.10).

### 4.2 The four-point cell-centered scheme

Let  $x_{i+1/2} = x_i + h_1/2$  and  $y_{j+1/2} = y_j + h_2/2$  for  $i = 0, 1, \dots, I-1$  and  $j = 0, 1, \dots, J-1$ . Let

$$T_{i+1/2,j+1/2} = \{(x,y) \mid |x - x_{i+1/2}| \leq h_1/2, |y - y_{j+1/2}| \leq h_2/2\}$$

be the cell centered at  $\mathbf{z}_{i+1/2,j+1/2} = (x_{i+1/2}, y_{j+1/2})$ . Denote the four edge centers by  $\mathbf{z}_{i+1,j+1/2}, \mathbf{z}_{i+1/2,j+1}, \mathbf{z}_{i,j+1/2}$  and  $\mathbf{z}_{i+1/2,j}$ .

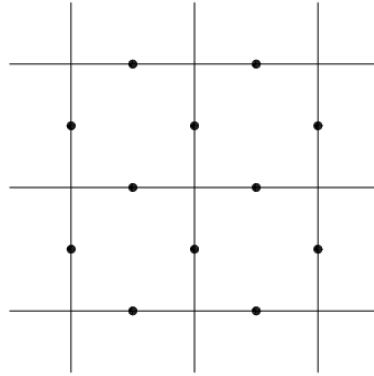


Figure 3: TFPM stencil for the four-point cell-centered scheme.

Once again, we assume the discrete ordinates equations (2.9) on  $T_{i+1/2,j+1/2}$  is approximated by the following first order partial differential equations with constant coefficients

$$\epsilon \left( c_m \frac{\partial}{\partial x} \tilde{\psi}_m + s_m \frac{\partial}{\partial y} \tilde{\psi}_m \right) + \sigma_T \tilde{\psi}_m = \epsilon^2 q + (\sigma_T - \epsilon^2 \sigma_a) \sum_{n \in V} \omega_n \tilde{\psi}_n, \quad \text{for } m \in V. \quad (4.8)$$

Let  $\Psi^{(0)} = (\psi_1^{(0)}, \dots, \psi_{4M}^{(0)})^T = \frac{q}{\sigma_a} (1, 1, \dots, 1)^T \in \mathbb{R}^{4M}$ . It is straightforward to check that  $\Psi^{(0)}$  is a particular solution of Eq. (4.8), and the difference  $\Psi(\mathbf{z}) = \tilde{\Psi}(\mathbf{z}) - \Psi^{(0)}$  satisfies the homogeneous equations

$$\epsilon \left( c_m \frac{\partial}{\partial x} \psi_m + s_m \frac{\partial}{\partial y} \psi_m \right) + \sigma_T \psi_m = (\sigma_T - \epsilon^2 \sigma_a) \sum_{n \in V} \omega_n \psi_n, \quad \text{for } m \in V. \quad (4.9)$$

Similar to the construction of the five-point node-centered scheme, let  $K$  be a positive integer, we consider  $K$  linearly independent solutions to Eq. (4.9)

$$\Psi^{(k)}(\mathbf{z}) = \zeta^{(k)} \exp \left\{ \frac{\lambda_k (x - x_{i+1/2}) + \mu_k (y - y_{j+1/2}) - \max\{\frac{1}{2}h_1|\lambda_k|, \frac{1}{2}h_2|\mu_k|\}}{\epsilon} \right\}, \quad (4.10)$$

for  $k = 1, 2, \dots, K$ . Here,  $(\lambda_k, \mu_k)$  is a real eigenvalue pair of equations (4.9) and  $\zeta^{(k)}$  is the eigenvector associated with  $(\lambda_k, \mu_k)$ .

**Remark 4.3.** (4.10) is the same as in (3.3) but subtracting  $(\lambda_k x_{i+1/2} + \mu_k y_{j+1/2} + \max\{\frac{1}{2}h_1|\lambda_k|, \frac{1}{2}h_2|\mu_k|\})/\epsilon$  in the power of the exponential, which is equivalent to multiplying some constant in the basis. We are interested in problems with a wide range of mean free paths, the constant subtracting in the exponential of (4.10) is to avoid overflow when  $\epsilon$  is small during computation.

Let  $\{\alpha_k, k = 1, 2, \dots, K\}$  be constants, It is obvious that the vector-valued function

$$\tilde{\Psi}(\mathbf{z}) = \Psi^{(0)} + \sum_{k=1}^K \alpha_k \Psi^{(k)}(\mathbf{z}) \quad (4.11)$$

is a solution of the nonhomogeneous system (4.8).

For each grid cell  $T_{i+1/2,j+1/2}$ , we choose the four edge centers

$$\{\mathbf{z}_{i+1,j+1/2}, \mathbf{z}_{i+1/2,j+1}, \mathbf{z}_{i,j+1/2}, \mathbf{z}_{i+1/2,j}\}$$

on the cell boundary  $\partial T_{i+1/2,j+1/2}$  to construct the discretization in the cell centered at  $\mathbf{z}_{i+1/2,j+1/2}$ .

The discrete in-flow boundary conditions for (4.8) are given by the  $K = 4 \times (4M/2) = 8M$  values at the four edge centers  $(\mathbf{z}_{i+1,j+1/2}, \mathbf{z}_{i+1/2,j+1}, \mathbf{z}_{i,j+1/2}, \mathbf{z}_{i+1/2,j})$ :

$$\begin{cases} \tilde{\psi}_m(\mathbf{z}_{i+1,j+1/2}), & \text{with } c_m < 0, \\ \tilde{\psi}_m(\mathbf{z}_{i+1/2,j+1}), & \text{with } s_m < 0, \\ \tilde{\psi}_m(\mathbf{z}_{i,j+1/2}), & \text{with } c_m > 0, \\ \tilde{\psi}_m(\mathbf{z}_{i+1/2,j}), & \text{with } s_m > 0, \end{cases} \quad (4.12)$$

for  $m \in V$ . Then the constants  $\{\alpha_k, k = 1, 2, \dots, K\}$  in (4.11) can be determined by the unknowns at the cell edges (4.12), namely, for  $m \in V$ ,

$$\begin{cases} \psi_m^{(0)} + \sum_{k=1}^K \alpha_k \psi_m^{(k)}(\mathbf{z}_{i+1,j+1/2}) = \tilde{\psi}_m(\mathbf{z}_{i+1,j+1/2}), & \text{with } c_m < 0, \\ \psi_m^{(0)} + \sum_{k=1}^K \alpha_k \psi_m^{(k)}(\mathbf{z}_{i+1/2,j+1}) = \tilde{\psi}_m(\mathbf{z}_{i+1/2,j+1}), & \text{with } s_m < 0, \\ \psi_m^{(0)} + \sum_{k=1}^K \alpha_k \psi_m^{(k)}(\mathbf{z}_{i,j+1/2}) = \tilde{\psi}_m(\mathbf{z}_{i,j+1/2}), & \text{with } c_m > 0, \\ \psi_m^{(0)} + \sum_{k=1}^K \alpha_k \psi_m^{(k)}(\mathbf{z}_{i+1/2,j}) = \tilde{\psi}_m(\mathbf{z}_{i+1/2,j}). & \text{with } s_m > 0. \end{cases} \quad (4.13)$$

This provides a system of  $8M$  linear algebraic equations. To determine the coefficients  $\{\alpha_k\}_{k=1}^K$ , same as the five-point scheme, we set  $K = 8M$ . From (4.11),

$$\begin{cases} \psi_m^{(0)} + \sum_{k=1}^K \alpha_k \psi_m^{(k)}(\mathbf{z}_{i+1,j+1/2}) = \tilde{\psi}_m(\mathbf{z}_{i+1,j+1/2}), & c_m > 0, \\ \psi_m^{(0)} + \sum_{k=1}^K \alpha_k \psi_m^{(k)}(\mathbf{z}_{i+1/2,j+1}) = \tilde{\psi}_m(\mathbf{z}_{i+1/2,j+1}), & s_m > 0, \\ \psi_m^{(0)} + \sum_{k=1}^K \alpha_k \psi_m^{(k)}(\mathbf{z}_{i,j+1/2}) = \tilde{\psi}_m(\mathbf{z}_{i,j+1/2}), & c_m < 0, \\ \psi_m^{(0)} + \sum_{k=1}^K \alpha_k \psi_m^{(k)}(\mathbf{z}_{i+1/2,j}) = \tilde{\psi}_m(\mathbf{z}_{i+1/2,j}), & s_m < 0. \end{cases} \quad (4.14)$$

After we express the constants  $\{\alpha_k, k = 1, 2, \dots, K\}$  by the unknowns in (4.12) through solving the system (4.13), substituting those expressions into (4.14) gives a finite difference scheme that connects together all unknowns at the four edge centers of the cell  $T_{i+1/2,j+1/2}$ . This is the four-point cell-centered tailored finite point scheme.

**Remark 4.4.** If one of the edge centers  $\{\mathbf{z}_{i+1,j+1/2}, \mathbf{z}_{i+1/2,j+1}, \mathbf{z}_{i,j+1/2}, \mathbf{z}_{i+1/2,j}\}$  is on the physical boundary  $\partial\mathbf{D}$  of the computational domain, we simply replace the corresponding component values  $\phi_m$  with the physical boundary conditions (2.10).

**Remark 4.5.** In order to determine  $\{\alpha_k\}_{k=1}^{8M}$  from (4.6) or (4.13), it is important that the coefficient matrix is not singular, which is the reason that we have to choose the special solutions, so that the eigenvalue pairs carefully. We use two groups of eigenvalue pairs, each of which has  $4M$  real eigenvalue pairs that satisfy  $\mu = \beta\lambda$  with  $\beta$  some constant. This choice is crucial to make the coefficient matrix for  $\{\alpha_k\}_{k=1}^{8M}$  nonsingular, which can be checked numerically. However, the analytical proof for this non singularity is still open and will be our future subject.

**Remark 4.6.** When programming, we can also set  $\{\alpha_k, k=1, \dots, 8M\}$  at each node (in each cell) as the unknowns and find the connections of  $\{\alpha_k\}_{k=1}^{8M}$  at different nodes (cell) by the continuity of  $\tilde{\Psi}(\mathbf{z})$  at the nodes (the cell edges).

## 5 Numerical examples

The performance of the five-point node-centered and four-point cell-centered TFPS are presented in this section. Here we have chosen the eigenvalue pairs on the coordinate axes of the  $\lambda\mu$ -plane, as described in Lemma 3.1. As we can see from Fig. 1, though the characteristic polynomial  $p_{4M}(\lambda, \mu)$  has  $4M$  distinct roots on each of the coordinate axes of the  $\lambda\mu$ -plane, when  $M$  increases, some of those  $4M$  distinct roots become too close to distinguish. This fact causes the coefficient matrixes in (4.6) or (4.13) become nearly singular. We can avoid this problem by using other quadrature sets. The question of how to choose the best quadrature set is an interesting and important problem but out of the scope of this present paper. Therefore, in the subsequent part, we have chosen the most used Gaussian quadrature and test the performance of our TFPS for  $M=1, 3, 6$ .

In all the examples, the computational domain is  $\Omega = [0, 1] \times [0, 1]$  and  $\Gamma$  denotes the boundary of  $\Omega$ . In those figures showing the numerical results of the four point cell centered TFPS, since only the values of the solution at the edge centers are known, we get the values at the cell center by averaging over all four edge centers and at the cell vertices by linear interpolation on the direction along which the solution has smaller slope.

**Example 5.1.** First we verify the accuracy and convergence order of both five-point node-centered scheme and four-point cell-centered scheme with different  $M$ 's ( $M=1, 3, 6$ ). We consider the homogeneous transport equation with

$$\sigma_T = 1; \quad \sigma_a = 1; \quad q = 0,$$

together with the Dirichlet boundary condition chosen in a way such that the exact solution to the Dirichlet BVP is

$$\Psi = \zeta^* \exp\{[\lambda^*(x-1) + \mu^*(y-1)]/\epsilon\} + \zeta^{**} \exp\{[\lambda^{**}(x-1) + \mu^{**}(y-1)]/\epsilon\}.$$

Here,  $(\lambda^*, \mu^*)$  and  $(\lambda^{**}, \mu^{**})$  are two eigenvalue pairs;  $\xi^*$  and  $\xi^{**}$  are the associated eigenvectors given by (3.9) or (3.12). We choose the eigenvalue pairs  $(\lambda^*, \mu^*)$  and  $(\lambda^{**}, \mu^{**})$ , respectively, to be the first and second intersection points of the characteristic curve in the first quadrant of the  $\lambda\mu$ -plane in Fig. 1 and the straight line that passes through the origin and has slope  $\tan(\pi/6)$ .

The discrete  $L^2$  norm of the numerical solutions for the node centered and cell centered TFPS are shown respectively in Tables 4 and 6. Here we have calculated the discrete error by comparing the numerical results and the exact values at the all nodes for the node centered scheme and all cell edge center for the cell centered scheme. We can see that, for all  $M = 1, 3, 6$ , when  $\epsilon$  is 0.2 and the mesh sizes are small, the node centered TFPS has first order convergence and the cell centered TFPS has second order accuracy. However, when  $\epsilon$  decreases, the convergence orders of both schemes decrease, Though the convergence order of the cell centered TFPS is higher than the node centered TFPS for all  $\epsilon$ , when  $\epsilon$  is too small, no convergence order can be observed for both schemes. This is because the exact solution under consideration exhibit a conner layer, when  $\epsilon$  is small, all the other parts are almost flat except the point (1,1). If the mesh is too coarse to "feel" the conner layer, the discrete errors are small, as we refine the mesh so that it can

Table 4: Example 5.1. The discrete  $L^2$  norm of the numerical error  $\|u - u_h\|_{L^2}$  by the five-point node-centered TFPS.

M	$\epsilon$	$8 \times 8$	$16 \times 16$	$32 \times 32$	$64 \times 64$	$128 \times 128$
1	2.00E-1	2.62E-2	2.49E-2	1.69E-2	9.65E-3	5.13E-3
	5.00E-2	1.49E-2	7.30E-3	7.97E-3	7.10E-3	4.66E-3
	2.00E-2	1.57E-2	7.86E-3	3.59E-3	3.14E-3	3.14E-3
	5.00E-3	1.58E-2	8.01E-3	4.07E-3	2.03E-3	9.18E-4
	2.00E-3	1.58E-2	8.01E-3	4.08E-3	2.06E-3	1.03E-3
	5.00E-4	1.59E-2	8.02E-3	4.08E-3	2.06E-3	1.04E-3
	2.00E-4	1.59E-2	8.02E-3	4.08E-3	2.06E-3	1.04E-3
3	2.00E-1	3.95E-2	2.83E-2	1.70E-2	9.40E-3	4.95E-3
	5.00E-2	3.93E-3	1.11E-2	1.16E-2	8.05E-3	4.77E-3
	2.00E-2	5.10E-4	9.88E-4	3.88E-3	5.02E-3	3.78E-3
	5.00E-3	5.12E-5	1.97E-5	1.39E-4	2.59E-4	9.94E-4
	2.00E-3	4.69E-5	1.34E-5	4.06E-6	3.18E-5	8.61E-5
	5.00E-4	4.48E-5	1.22E-5	3.26E-6	8.81E-7	3.29E-7
	2.00E-4	4.44E-5	1.20E-5	3.14E-6	8.19E-7	2.49E-7
6	2.00E-1	3.72E-3	2.24E-3	1.26E-3	6.71E-4	3.45E-4
	5.00E-2	1.08E-3	4.54E-4	2.88E-4	1.71E-4	9.34E-5
	2.00E-2	1.00E-3	1.81E-4	8.61E-5	5.80E-5	3.56E-5
	5.00E-3	1.07E-3	1.49E-4	2.24E-5	8.16E-6	6.84E-6
	2.00E-3	1.10E-3	1.52E-4	2.05E-5	3.31E-6	1.61E-6
	5.00E-4	1.11E-3	1.55E-4	2.07E-5	2.78E-6	4.62E-7
	2.00E-4	1.11E-3	1.56E-4	2.09E-5	2.78E-6	4.26E-7

Table 5: Example 5.1. The extended discrete  $L^2$  norm of the numerical error  $\|u - u_h\|_{\ell^2}$  by the five-point node-centered TFPS.

$M$	$\epsilon$	$8 \times 8$	$16 \times 16$	$32 \times 32$	$64 \times 64$	$128 \times 128$
1	2.00E-1	4.18E-2	2.59E-2	1.56E-2	8.87E-3	4.71E-3
	2.00E-2	4.00E-3	2.92E-3	2.74E-3	3.35E-3	2.65E-3
	2.00E-3	2.58E-3	6.51E-4	1.67E-4	4.61E-5	1.65E-5
	2.00E-4	2.58E-3	6.50E-4	1.67E-4	4.56E-5	1.53E-5
3	2.00E-1	6.52E-2	3.00E-2	1.62E-2	8.88E-3	4.70E-3
	2.00E-2	3.47E-2	2.79E-2	1.62E-2	7.46E-3	3.38E-3
	2.00E-3	2.58E-3	6.54E-4	1.76E-4	9.22E-5	1.21E-4
	2.00E-4	2.58E-3	6.50E-4	1.67E-4	4.56E-5	1.53E-5
6	2.00E-1	4.95E-3	2.24E-3	1.18E-3	6.29E-4	3.27E-4
	2.00E-2	2.64E-3	7.06E-4	2.12E-4	7.71E-5	3.45E-5
	2.00E-3	2.58E-3	6.51E-4	1.67E-4	4.61E-5	1.57E-5
	2.00E-4	2.58E-3	6.50E-4	1.67E-4	4.56E-5	1.53E-5

Table 6: Example 5.1. The discrete  $L^2$  norm of the numerical errors  $\|u - u_h\|_{\ell^2}$  by the four-point cell-centered TSPS.

$M$	$\epsilon$	$8 \times 8$	$16 \times 16$	$32 \times 32$	$64 \times 64$	$128 \times 128$
1	2.00E-1	2.58E-3	7.07E-4	1.80E-4	4.50E-5	1.12E-5
	5.00E-2	3.22E-3	2.28E-3	7.86E-4	2.10E-4	5.29E-5
	2.00E-2	2.61E-4	1.18E-3	1.19E-3	4.76E-4	1.33E-4
	5.00E-3	5.74E-5	2.57E-5	5.62E-5	3.05E-4	3.02E-4
	2.00E-3	2.91E-5	1.24E-5	5.50E-6	7.87E-6	8.93E-5
	5.00E-4	1.86E-5	5.47E-6	1.95E-6	1.03E-6	1.08E-6
	2.00E-4	1.78E-5	4.76E-6	1.99E-6	2.30E-6	3.47E-6
3	2.00E-1	1.22E-2	3.44E-3	8.91E-4	2.25E-4	5.66E-5
	5.00E-2	1.56E-2	9.65E-3	3.36E-3	9.23E-4	2.36E-4
	2.00E-2	3.98E-3	6.39E-3	5.02E-3	1.99E-3	5.72E-4
	5.00E-3	6.21E-5	3.55E-4	1.04E-3	1.64E-3	1.27E-3
	2.00E-3	2.94E-5	1.28E-5	7.44E-5	3.31E-4	6.01E-4
	5.00E-4	1.86E-5	5.49E-6	1.98E-6	1.10E-6	1.88E-5
	2.00E-4	1.78E-5	4.72E-6	1.87E-6	2.01E-6	1.75E-7
6	2.00E-1	8.21E-4	2.29E-4	5.93E-5	1.50E-5	3.75E-6
	5.00E-2	3.84E-4	1.58E-4	5.14E-5	1.40E-5	3.59E-6
	2.00E-2	1.89E-4	8.42E-5	3.66E-5	1.31E-5	3.74E-6
	5.00E-3	5.97E-5	2.79E-5	1.27E-5	6.32E-6	3.62E-6
	2.00E-3	2.95E-5	1.28E-5	5.87E-6	2.80E-6	1.74E-6
	5.00E-4	1.86E-5	5.50E-6	1.98E-6	1.00E-6	9.62E-7
	2.00E-4	1.78E-5	4.74E-6	1.81E-6	2.09E-6	1.69E-7

Table 7: Example 5.1. The extended discrete  $L^2$  norm of the numerical errors  $\|u - u_h\|_{\ell^2}$  by the four-point cell-centered TSPS.

$M$	$\epsilon$	$8 \times 8$	$16 \times 16$	$32 \times 32$	$64 \times 64$	$128 \times 128$
1	2.00E-1	1.49E-2	4.40E-3	1.21E-3	3.55E-4	1.30E-4
	2.00E-2	5.09E-3	4.50E-3	3.41E-3	1.85E-3	9.00E-4
	2.00E-3	6.53E-4	1.65E-4	4.26E-5	1.57E-5	1.05E-4
	2.00E-4	6.52E-4	1.64E-4	4.20E-5	1.19E-5	6.23E-6
3	2.00E-1	1.84E-2	4.89E-3	1.25E-3	3.19E-4	8.34E-5
	2.00E-2	3.31E-2	1.94E-2	8.27E-3	2.70E-3	7.73E-4
	2.00E-3	9.43E-4	6.96E-4	6.75E-4	6.63E-4	6.03E-4
	2.00E-4	6.52E-4	1.64E-4	4.20E-5	1.18E-5	3.80E-6
6	2.00E-1	1.07E-3	2.81E-4	7.35E-5	2.07E-5	6.95E-6
	2.00E-2	7.05E-4	2.02E-4	6.21E-5	1.98E-5	6.96E-6
	2.00E-3	6.53E-4	1.65E-4	4.27E-5	1.23E-5	4.62E-6
	2.00E-4	6.52E-4	1.64E-4	4.20E-5	1.18E-5	3.79E-6

"feel" the fast changes at the layer, the discrete errors increase. Yet this does not indicate the coarse meshes give better approximations, it is due to the way of computing the discrete errors. If, instead of using only those values at the nodes (edge centers) to get the discrete errors for the coarse mesh, we find all those values at the nodes (edge centers) of the finest mesh by interpolations, comparing which with the exact solution, we can get an extended discrete error. The interpolation method around each node (inside each cell) is straightforward, after getting  $\{\alpha_k\}, k=1, \dots, 8M$  from (4.6), (4.13), the solution can be locally approximated by the linear combination of basis functions. The interpolation values can be different by the basis of different nodes and we compute their average.

In Tables 5 and 7, the discrete errors calculated using those extended values at  $256 \times 256$  meshes are presented. From Fig. 4, uniform convergence can be observed for both

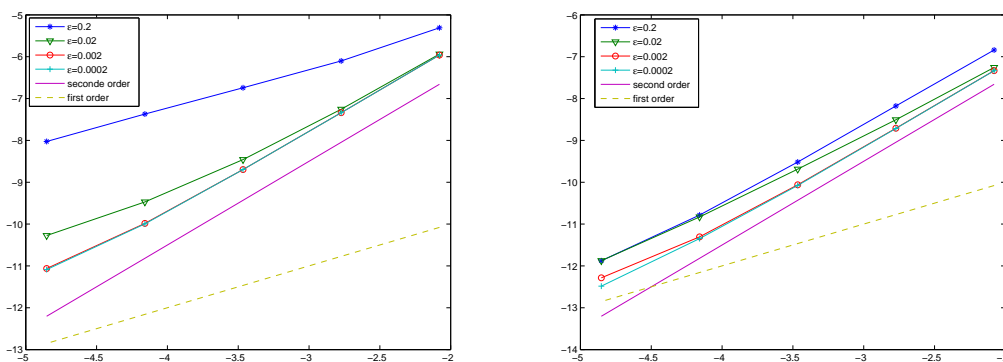


Figure 4: Example 5.1. Numerical convergence order of the extended discrete errors given in Tables 5 and 7 for  $M=6$ . Left: five point node centered scheme; right: four point cell centered scheme.

TFPS, especially, the four point cell centered TFPS possesses uniform second order convergence.

**Example 5.2.** Let

$$\sigma_T(x,y) = 1; \quad \sigma_a = 1; \quad q(x,y) = 1.$$

First of all, we check numerically that the diffusion limit can be captured by using isotropic boundary conditions. For different  $\epsilon = 0.1$  and  $\epsilon = 0.0001$ , the numerical results of using isotropic boundary conditions  $\psi_m|_\Gamma = 0$ , are presented in Figs. 5 and 6. We can see that even if  $\epsilon$  is much smaller than the mesh size, the solution of the diffusion limit equation can be captured by TFPS.

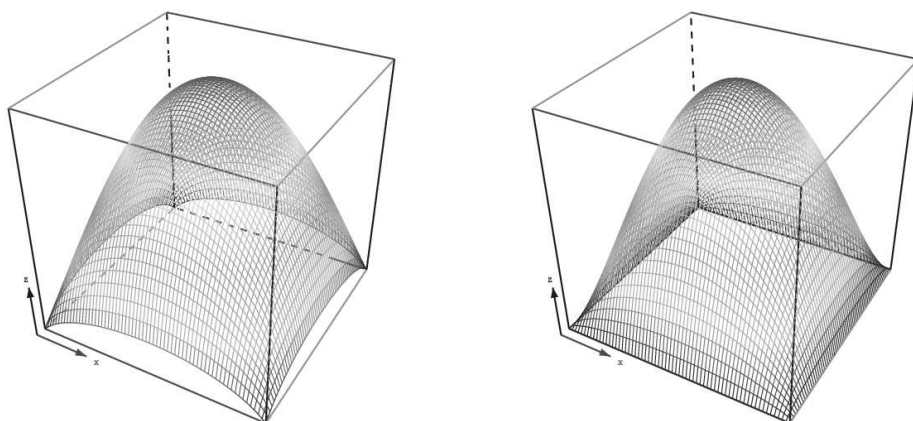


Figure 5: Example 5.2. Numerical solution to a problem with the isotropic and homogeneous boundary condition by the five-point node-centered scheme ( $M=6$ ) with different diffusion parameters: left:  $\epsilon=0.1$ ; right:  $\epsilon=0.0001$ .

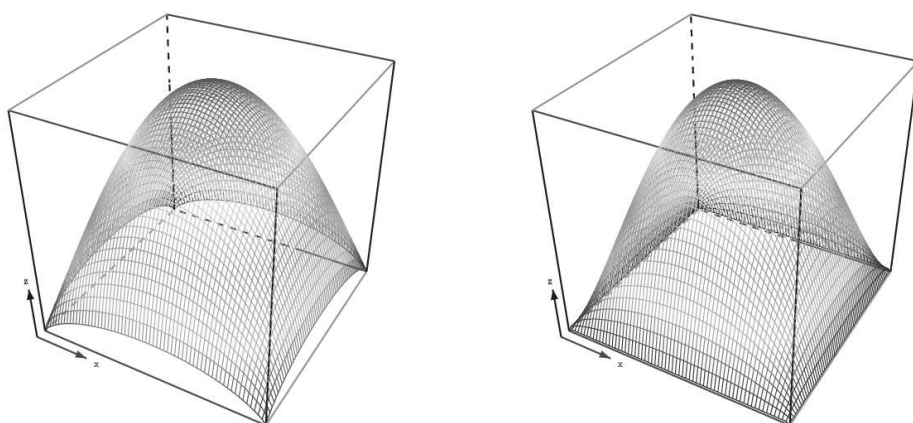


Figure 6: Example 5.2. Numerical solution to a problem with the isotropic and homogeneous boundary condition by the four-point scheme ( $M=6$ ) with different diffusion parameters: left:  $\epsilon=0.1$ ; right:  $\epsilon=0.0001$ . Here we have used  $h_1=h_2=1/32$ .

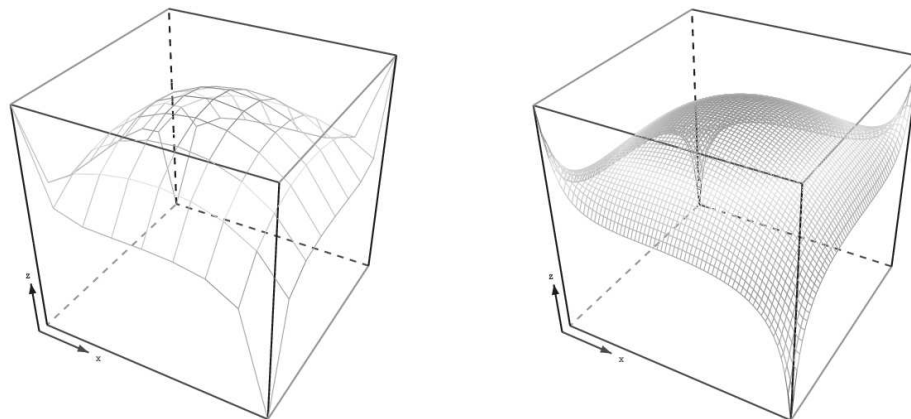


Figure 7: Example 5.2. Numerical solution with boundary layers by the five-point node-centered scheme with  $M=6$ ,  $\epsilon=0.1$ . Left: grid size  $1/8$ ; right: grid size  $1/64$ .

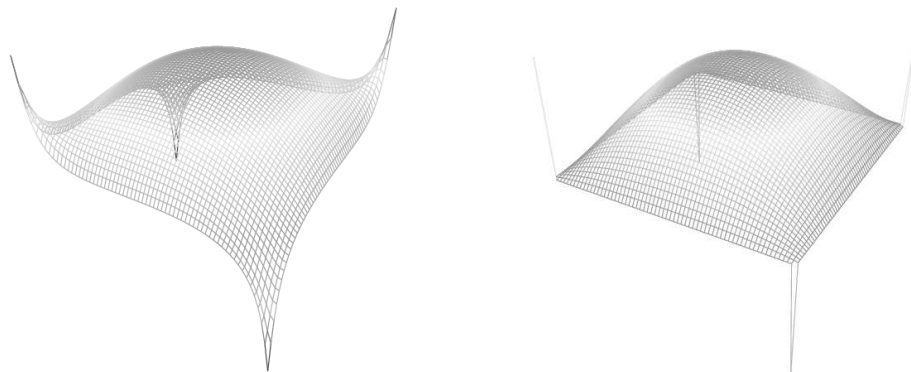


Figure 8: Example 5.2. Numerical solution with boundary layers by the five-point node-centered scheme with  $M=6$ : left:  $\epsilon=0.1$ ; right:  $\epsilon=0.001$ .

When the injected particle densities are anisotropic such that

$$\psi_m = \begin{cases} 0, & \text{if } c_m s_m > 0, \\ 1, & \text{if } c_m s_m < 0. \end{cases}$$

We can see from Figs. 7 and 9 that boundary layers appear and both TFPS can capture the layers by coarse mesh. Especially, in Figs. 8 and 10, when  $\epsilon$  becomes small, the fast change can be seen even if there is only one node in the layer.

**Example 5.3.** We show an example that the coefficients vary with space and have discontinuous at the interfaces. The computational domain  $\Omega$  is composed of two parts  $\Omega_1 = [0,0.5] \times [0,0.5]$  and  $\Omega_2 = [0,0.5] \times (0.5,1] \cup (0.5,1] \times [0,1]$ .  $\Omega_1$  is a transport region with

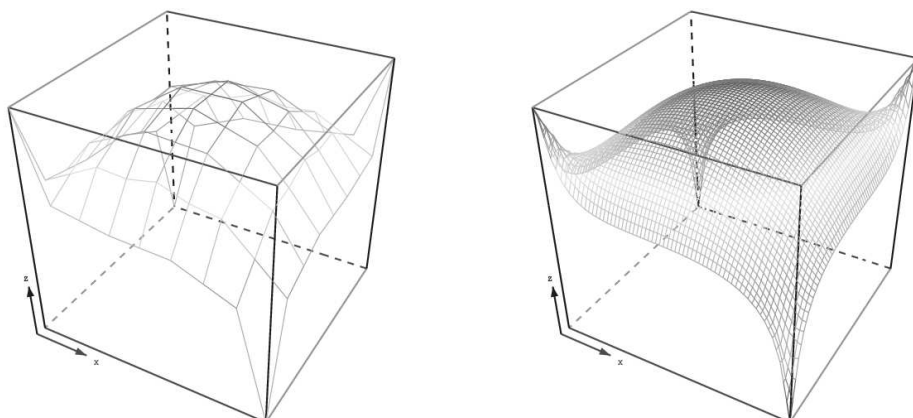


Figure 9: Example 5.2. Numerical solution with boundary layers by the four-point cell-centered scheme with  $M=6$ ,  $\epsilon=0.1$  on different grids: left: grid size  $1/4$ ; right: grid size  $1/32$ . Here we have used  $h_1=h_2=1/32$ .

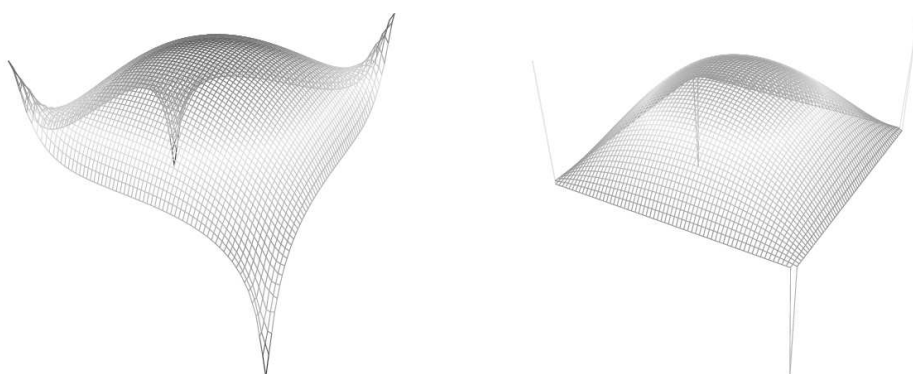


Figure 10: Example 5.2. Numerical solution with boundary layers by the four-point cell-centered scheme with  $M=6$ : left:  $\epsilon=0.1$ ; right:  $\epsilon=0.001$ .

$\epsilon$  at  $\mathcal{O}(1)$  while  $\Omega_2$  is a diffusion region with  $\epsilon$  very small.

$$\begin{aligned} \text{On } \Omega_1: & \quad \sigma_T = 1 + 10(x^2 + y^2), \quad \sigma_a = 1 + 10(x^2 + y^2), \quad q = 5, \quad \epsilon = 0.5; \\ \text{On } \Omega_2: & \quad \sigma_T = 11, \quad \sigma_a = 5, \quad q = 0, \quad \epsilon = 0.001. \end{aligned}$$

The boundary conditions are anisotropic such that

$$\psi_m = \begin{cases} 0, & \text{if } c_m s_m > 0, \\ 1, & \text{if } c_m s_m < 0. \end{cases}$$

The numerical results using the quadrature set  $S_4$  ( $M=6$ ) calculated with different meshes are presented in Fig. 11. We can see that both boundary and interface layers exist. Fig. 12 presents those values at the cross section  $x=1/4$  calculated with different meshes. The fast changes in the layers can be captured quite well by very coarse mesh.

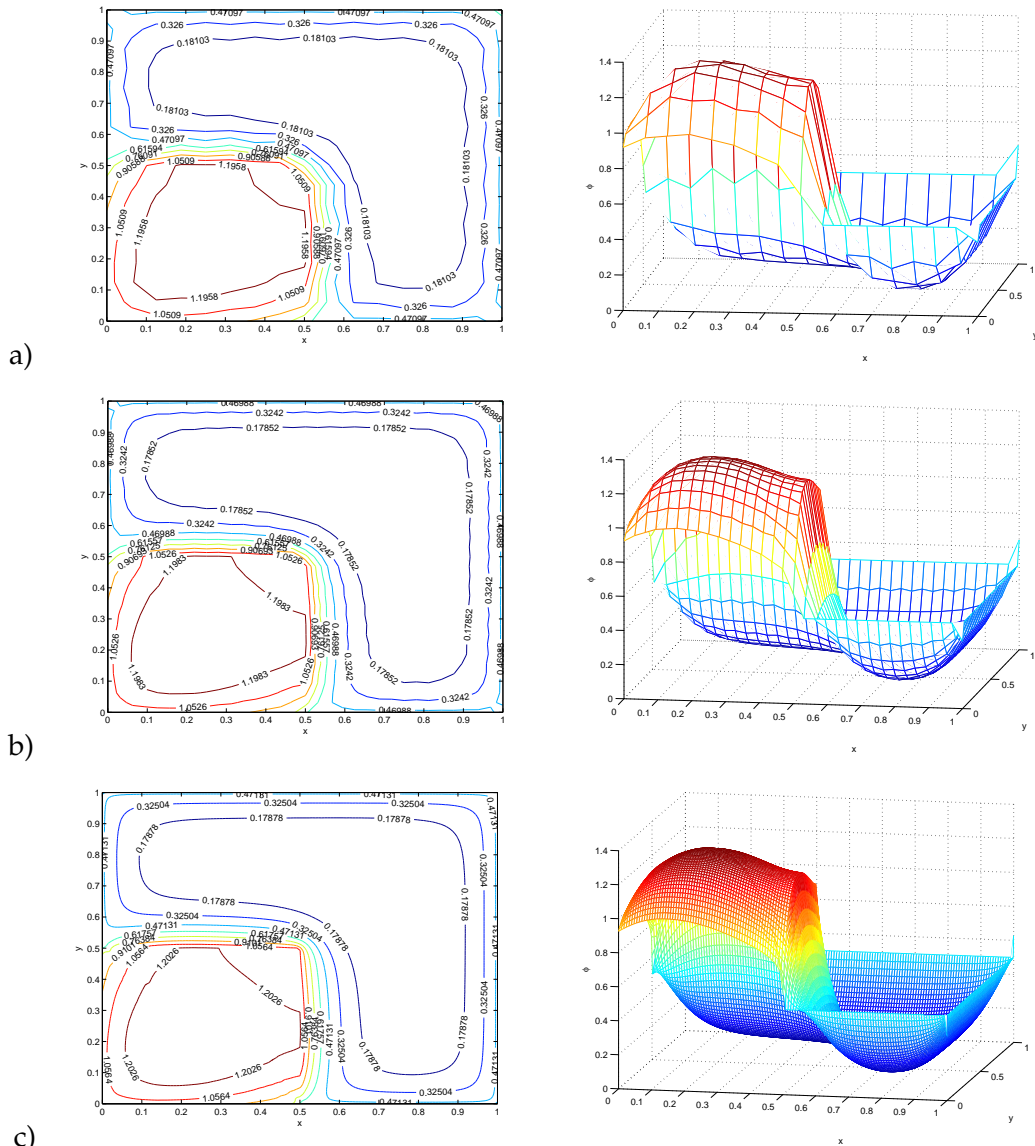


Figure 11: Example 5.3. The numerical results of different meshes. The left column is the contour plot while the right column depicts the values of  $\phi(x,y)$ . a)  $h_1 = h_2 = 1/8$ ; b)  $h_1 = h_2 = 1/16$ ; c)  $h_1 = h_2 = 1/64$ .

## 6 Discussion

This paper presents two uniformly convergent numerical schemes for the steady state discrete ordinates neutron or radiative transport equation. The idea of the five-point node-centered TFPS is that, firstly, approximate the coefficients  $\sigma_T$ ,  $\sigma_a$  and  $q$  in the four cells around each node by constants, and then locally express the solution by a linear

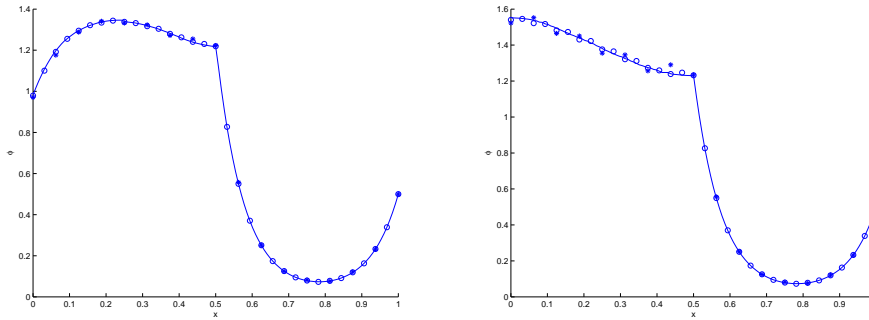


Figure 12: Example 5.3. The numerical results at the cross section  $x=1/4$  calculated with different meshes. Here we have used the four point cell centered TFPS with  $M=6$ . The stars, circles and solid lines are respectively the numerical results of  $h_1=h_2=1/8$ ,  $h_1=h_2=1/16$  and  $h_1=h_2=1/64$ . Left:  $\phi$ ; right:  $\psi_6$ .

combination of special solutions of the constant coefficient equation, using which to formulate a linear system for the unknown variables at the four neighboring nodes. The idea of the four-point cell-centered TFPS resembles the finite element method, but the basis functions in each cell are chosen to be the special solutions of constant coefficient equation and we piece together the numerical solution with the neighboring cells by the interface conditions at the cell edge centers.

Numerical examples show that the five-point scheme has first-order accuracy and the four-point scheme has second-order accuracy. Both schemes can capture not only the diffusion limit under isotropic boundary conditions when the mean free path tends to zero, but also the boundary layers without resolving the fast changes, for problems with anisotropic boundary conditions. Furthermore, the four-point cell-centered TFPS can be applied to problems with discontinuous coefficients. We can use coarse meshes to capture the interface condition of the diffusion limit equation as well as the fast changes in the interface layers.

In this paper, we only present the construction of two TFPS, demonstrate their uniform convergence and ability to capture the layers numerically. There are several interesting theoretical questions worth investigating. For example, the characteristic curves in Fig. 1 contain a lot of information about the layer structure and may shed some light to understand the ray effect [22]. It is quite crucial to choose those eigenvalue pairs on the  $x$  and  $y$  axes, which relates to the rectangular meshes we use, but the explanation is open and will be our future subject. Furthermore, the extension of the TFPS to three dimensional is straight forward and we will extend this method to more general meshes and collision kernels.

## Acknowledgments

H. Han is supported by the NSFC Project No. 10971116. M. Tang is supported by Natural Science Foundation of Shanghai under Grant No. 12ZR1445400 and Shanghai Pujiang

Program 13PJ1404700. W. Ying was supported in part by the National Natural Science Foundation of China under Grant DMS-11101278 and the Young Thousand Talents Program of China.

The authors would like to thank Prof. G. Bal for his useful suggestions and comments.

## References

- [1] M. L. Adams, Discontinuous finite element transport solutions in thick diffusive problems, *Nucl. Sci. Eng.*, 137 (2001), 298–333.
- [2] F. Anli and S. Güngör, A spectral nodal method for one-group  $x,y,z$ -cartesian geometry discrete ordinates problems, *Annals of Nuclear Energy*, 23 (1996), 669–680.
- [3] Y. Y. Azmy, Arbitrarily high order characteristic methods for solving the neutron transport equation, *Ann. Nucl. Energy*, 19 (1992), 593–606.
- [4] G. Bal and L. Ryzhik, Diffusion Approximation of Radiative Transfer Problems with Interfaces, *SIAM, J. Appl. Math.*, 60(6) (2000), 1887–1912.
- [5] R.C. De Barros and E.W. Larsen, A numerical method for one-group slab-geometry discrete ordinates problems with no spatial truncation error, *Nuclear Science and Engineering*, 104 (1990), 199–208.
- [6] R.C. De Barros and E.W. Larsen, A spectral nodal method for one-group  $x,y$ -geometry discrete ordinates problems, *Nuclear Science and Engineering*, 111 (1992), 34–45.
- [7] C. R. Brennan, R. L. Miller, K. A. Mathews, Split-cell exponential characteristic transport method for unstructured tetrahedral meshes, *Nucl. Sci. Eng.*, 138 (2001), 26–44.
- [8] S. Jin, Asymptotic preserving (ap) schemes for multiscale kinetic and hyperbolic equations: a review. lecture notes for summer school on “methods and models of kinetic theory” (mmkt), tech. report, *Rivista di Matematica della Università di Parma, Porto Ercole (Grosseto, Italy)*, 2010.
- [9] S. Jin, M. Tang and H. Han, A uniformly second order numerical method for the one-dimensional discrete-ordinate transport equation and its diffusion limit with interface, *Networks and Heterogeneous Media*, 4, (2009), 35–65.
- [10] S. Jin, X. Yang and G. W. Yuan, A domain decomposition method for a two-scale transport equation with energy flux conserved at the interface, *Kinetic and Related Models*, 1, (2008), 65–84.
- [11] H. Han, J.J.H. Miller and M. Tang, A parameter-uniform tailored finite point method for singularly perturbed linear ODE systems, *J. Comp. Math.*, 31 (2013), 422–438.
- [12] H. Han and Z. Huang, A tailored finite point method for the Helmholtz equation with high wave numbers in heterogeneous medium, *J. Comp. Math.*, 26 (2008), 728–739.
- [13] H. Han and Z. Huang, Tailored finite point method for a singular perturbation problem with variable coefficients in two dimensions, *Journal of Scientific Computing*, 41 (2009), 200–220.
- [14] H. Han and Z. Huang, Tailored finite point method for steady-state reaction-diffusion equations, *Commun. Math. Sci.*, 8 (2010), 887–899.
- [15] H. Han, Z. Huang, and R. B. Kellogg, The tailored finite point method and a problem of P. Hemker, in *Proceedings of International Conference on Boundary and Interior Layers – Computational and Asymptotic Methods*, 2008.
- [16] H. Han, Z. Huang, and R. B. Kellogg, A tailored finite point method for a singular perturbation problem on an unbounded domain, *Journal of Scientific Computing*, 36 (2008), 243–261.

- [17] P.-W. Hsieh, Y. Shih and S.-Y. Yang, A tailored finite point method for solving steady MHD duct flow problems with boundary layers, *Commun. Comput. Phys.*, 10 (2011), 161–182.
- [18] Z. Huang and X. Yang, Tailored finite cell method for solving Helmholtz equation in layered heterogeneous medium, *J. Comput. Math.*, 30(4), (2012), 381–391.
- [19] E. W. Larsen, J. E. Morel, and W. F. Miller Jr., Asymptotic solutions of numerical transport problems in optically thick, diffusive regimes, *J. Comput. Phys.*, 69 (1987), 283–324.
- [20] E. W. Larsen and J. E. Morel, Asymptotic solutions of numerical transport problems in optically thick, diffusive regimes II, *J. Comput. Phys.*, 83 (1989), 212–236.
- [21] E. W. Larsen, The asymptotic diffusion limit of discretized transport problems. *Nucl. Sci. Eng.*, 112 (1992), 336–346, (review).
- [22] E. W. Larsen and J. E. Morel, *Advances in Discrete-Ordinates Methodology*, in *Nuclear Computational Science: A Century in Review*, edited by Y. Y. Azmy and E. Sartori, Springer-Verlag, Berlin. (2010).
- [23] R. D. Lawrence, Progress in nodal methods for the solution of the neutron diffusion and transport equations. *Prog. Nucl. Energy*, 17, (1986), 271 (review).
- [24] E. E. Lewis and W.F. Miller, Jr. *Computational Methods of Neutron Transport*. John Wiley and Sons, New York, (1984).
- [25] M. Lemou and F. Mehats, Micro-macro schemes for kinetic equations including boundary layers, *SIAM J. Sci. Comput.* 34(6) (2012), 734–760.
- [26] Y. Shih, R. B. Kellogg, and Y. Chang, Characteristic tailored finite point method for convection-dominated convection-diffusion-reaction problems, *Journal of Scientific Computing*, 47 (2011), 198–215.
- [27] Y. Shih, R. B. Kellogg, and P. Tsai, A tailored finite point method for convection-diffusion-reaction problems, *Journal of Scientific Computing*, 43 (2010), 239–260.
- [28] M. Tang, A uniform first order method for the discrete ordinate transport equation with interfaces in X,Y-geometry. *Journal of Computational Mathematics*, 27 (2009), 764–786.
- [29] J.S. Warsa, T. A. Wareing, J.E. Morel, Fully consistent diffusion synthetic acceleration of linear discontinuous SN transport discretizations on unstructured tetrahedral meshes. *Nucl. Sci. Eng.*, 141 (2002), 236–251.